JGR Atmospheres

RESEARCH ARTICLE
10.1029/2025JD046135

Multi-Model Impacts of Dust on African Air Quality and Mortality Under Regional and Global Anthropogenic Aerosol Changes

Joe Adabouk Amooli[1], Ron L. Miller[2,3], Kostas Tsigaridis[2,3], Sourangsu Chowdhury[4], Yanda Zhang[1], Catherine A. Toolan[5], Sharar Ahmadi[6], Robert J. Allen[7], Maxwell T. Elling[8,9], Annica M. L. Ekman[10], Luke Fraser-Leach[11], Paul Griffiths[12], James Keeble[13], Tsuyoshi Koshiro[14], Paul Kushner[11], Anna Lewinschal[10], Marianne T. Lund[4], Molly MacRae[15], Risto Makkonen[16], Joonas Merikanto[16], Larissa Nazarenko[3], Pierre Nabat[17], Declan O'Donnell[16], Naga Oshima[14], Geeta Persad[18], Steven T. Rumbold[6], Knut von Salzen[19], Bjørn H. Samset[4,5], Neil C. Swart[19], Toshihiko Takemura[20], Laura J. Wilcox[5,6], and Daniel M. Westervelt[1]

[1]Lamont-Doherty Earth Observatory, Columbia University, New York, NY, USA, [2]Center for Climate Systems Research, Columbia University, New York, NY, USA, [3]NASA Goddard Institute for Space Studies, New York, NY, USA, [4]CICERO Center for International Climate Research, Oslo, Norway, [5]Department of Meteorology, University of Reading, Reading, UK, [6]National Centre for Atmospheric Science, University of Reading, Reading, UK, [7]University of California Riverside, Riverside, CA, USA, [8]Department of Atmospheric and Oceanic Sciences, University of Colorado Boulder, Boulder, CO, USA, [9]Cooperative Institute for Research in Environmental Sciences, University of Colorado Boulder, Boulder, CO, USA, [10]Department of Meteorology, Bolin Centre for Climate Research, Stockholm University, Stockholm, Sweden, [11]Department of Physics, University of Toronto, Toronto, ON, Canada, [12]School of Chemistry, University of Bristol, Bristol, UK, [13]Lancaster Environment Centre, Lancaster University, Lancaster, UK, [14]Meteorological Research Institute, Japan Meteorological Agency, Ibaraki, Japan, [15]Rutherford Appleton Laboratory, Centre for Environmental Data Analysis, Didcot, UK, [16]Finnish Meteorological Institute, Helsinki, Finland, [17]Météo-France, CNRS, University Toulouse, CNRM, Toulouse, France, [18]Jackson School of Geosciences, The University of Texas at Austin, Austin, TX, USA, [19]Canadian Centre for Climate Modelling and Analysis, Environment and Climate Change Canada, Victoria, BC, Canada, [20]Research Institute for Applied Mechanics, Kyushu University, Fukuoka, Japan

Abstract Decreases in anthropogenic aerosols will reduce fine particulate matter ($PM_{2.5}$); however, meteorological feedbacks alter dust emissions, modifying air quality gains. We use eight Earth System Models from the Regional Aerosol Model Intercomparison Project (RAMIP) simulations to assess African climate and air quality responses to anthropogenic aerosol emission perturbations, including meteorological feedbacks on dust emissions. By 2050, African and global emissions reductions drive the largest continent-average $PM_{2.5}$ decrease (0.92 ± 0.17 μg m^{-3}; 5% and 1.35 ± 0.50 μg m^{-3}; 7%, respectively) relative to SSP3-7.0, though regional dust increases partially offset these reductions. Anthropogenic emissions reductions in the U.S. and Europe also lower African $PM_{2.5}$ by 0.29 ± 0.32 μg m^{-3} (2%) due to teleconnections of Northern Hemisphere warming influencing the Intertropical Convergence Zone. Inter-model variability in dust and total $PM_{2.5}$ reflects differences in meteorological responses and dust emission parameterizations. Meteorological responses explain 90% of dust emissions variability across regions. Aerosol-driven climate feedbacks on dust account for up to 70% of total $PM_{2.5}$ changes in the Sahara and Namib, offsetting up to 20% of anthropogenic $PM_{2.5}$ reductions across Africa. Under 2050 global and Africa-wide anthropogenic aerosol reductions, 96,000 (95% CI: 54,000–137,000) and 84,000 (95% CI: 43,000–125,000) $PM_{2.5}$-related deaths are avoided in Africa, respectively. Dust $PM_{2.5}$ contributes an uncertain 3.4% of the avoided deaths under global reductions and has no net effect under Africa-wide reductions. Aerosol-driven climate feedbacks may partially offset direct air quality gains, though their continental-scale contribution remains small and uncertain.

Plain Language Summary Future reductions in human-caused aerosol emissions are expected to lower the concentrations of $PM_{2.5}$ (fine particles smaller than 2.5 μm), but climate responses from the reductions can also alter natural dust emissions, which may offset or enhance these improvements. Using climate model simulations, we examined how reductions in regional and global human-caused emissions affect African air quality, including the role of climate-driven changes in dust. By 2050, reductions in African and global human-caused emissions lead to the largest decreases in $PM_{2.5}$ across the continent. Human-caused emission reductions in the United States and Europe also reduce $PM_{2.5}$ in Africa by modifying large-scale atmospheric circulation and long-range transport of pollution. In the Sahara and Namib deserts, changes in dust accounts for up to 70%

Key Points:

- Global and Africa-wide anthropogenic aerosol emission reductions would avoid 96,000 and 84,000 $PM_{2.5}$-related deaths per year in Africa
- Dust feedbacks may modify the magnitude of air quality gains from regional and global anthropogenic aerosol emission reductions
- Wind gustiness is the dominant driver of dust emission changes resulting from anthropogenic aerosol emission reductions

Supporting Information:

Supporting Information may be found in the online version of this article.

Correspondence to:

D. M. Westervelt,
danielmw@ldeo.columbia.edu

Citation:

Amooli, J. A., Miller, R. L., Tsigaridis, K., Chowdhury, S., Zhang, Y., Toolan, C. A., et al. (2026). Multi-model impacts of dust on African air quality and mortality under regional and global anthropogenic aerosol changes. *Journal of Geophysical Research: Atmospheres*, *131*, e2025JD046135. https://doi.org/10.1029/2025JD046135

Received 11 DEC 2025
Accepted 23 APR 2026

Author Contributions:

Conceptualization: Joe Adabouk Amooli, Ron L. Miller, Kostas Tsigaridis, Sharar Ahmadi, Robert J. Allen, Annica M. L. Ekman, Paul Griffiths, Marianne T. Lund, Bjørn H. Samset, Neil C. Swart, Laura J. Wilcox, Daniel M. Westervelt
Data curation: Joe Adabouk Amooli, Ron L. Miller, Kostas Tsigaridis, Sourangsu Chowdhury, Yanda Zhang, Catherine A. Toolan, Sharar Ahmadi, Robert J. Allen, Maxwell T. Elling, Annica M. L. Ekman, Luke Fraser-Leach, Paul Griffiths, James Keeble,

Tsuyoshi Koshiro, Paul Kushner, Anna Lewinschal, Marianne T. Lund, Molly MacRae, Risto Makkonen, Joonas Merikanto, Larissa Nazarenko, Pierre Nabat, Declan O'Donnell, Naga Oshima, Geeta Persad, Steven T. Rumbold, Knut von Salzen, Bjørn H. Samset, Neil C. Swart, Toshihiko Takemura, Laura J. Wilcox, Daniel M. Westervelt

Formal analysis: Joe Adabouk Amooli, Sourangsu Chowdhury, Luke Fraser-Leach, Neil C. Swart, Daniel M. Westervelt

Funding acquisition: Joe Adabouk Amooli, Daniel M. Westervelt

Investigation: Joe Adabouk Amooli, Ron L. Miller, Kostas Tsigaridis, Sharar Ahmadi, Robert J. Allen, Annica M. L. Ekman, Paul Griffiths, Marianne T. Lund, Bjørn H. Samset, Neil C. Swart, Laura J. Wilcox, Daniel M. Westervelt

Methodology: Joe Adabouk Amooli, Ron L. Miller, Kostas Tsigaridis, Sourangsu Chowdhury, Yanda Zhang, Sharar Ahmadi, Robert J. Allen, Maxwell T. Elling, Annica M. L. Ekman, Luke Fraser-Leach, Paul Griffiths, Marianne T. Lund, Bjørn H. Samset, Neil C. Swart, Laura J. Wilcox, Daniel M. Westervelt

Project administration: Joe Adabouk Amooli, Ron L. Miller, Kostas Tsigaridis, Sharar Ahmadi, Robert J. Allen, Paul Griffiths, Marianne T. Lund, Bjørn H. Samset, Laura J. Wilcox, Daniel M. Westervelt

Resources: Joe Adabouk Amooli, Ron L. Miller, Kostas Tsigaridis, Sourangsu Chowdhury, Yanda Zhang, Catherine A. Toolan, Sharar Ahmadi, Robert J. Allen, Paul Griffiths, Paul Kushner, Marianne T. Lund, Knut von Salzen, Bjørn H. Samset, Neil C. Swart, Laura J. Wilcox, Daniel M. Westervelt

Software: Joe Adabouk Amooli, Kostas Tsigaridis, Sharar Ahmadi, Paul Griffiths, Neil C. Swart, Laura J. Wilcox, Daniel M. Westervelt

Supervision: Joe Adabouk Amooli, Daniel M. Westervelt

Validation: Joe Adabouk Amooli, Ron L. Miller, Kostas Tsigaridis, Sourangsu Chowdhury, Yanda Zhang, Maxwell T. Elling, Annica M. L. Ekman, Luke Fraser-Leach, Paul Griffiths, Neil C. Swart, Daniel M. Westervelt

Visualization: Joe Adabouk Amooli, Catherine A. Toolan, Neil C. Swart, Toshihiko Takemura, Daniel M. Westervelt

Writing – original draft: Joe Adabouk Amooli, Neil C. Swart, Daniel M. Westervelt

Writing – review & editing: Joe Adabouk Amooli, Ron L. Miller, Kostas Tsigaridis, Sourangsu Chowdhury, Yanda Zhang, Catherine A. Toolan, Sharar Ahmadi, Robert J. Allen, Maxwell T. Elling, Annica M. L. Ekman, Luke Fraser-Leach, Paul Griffiths,

of total $PM_{2.5}$ changes, while in West and East Africa, climate-driven increases in dust can offset up to 20% of air quality improvements. Overall, global and Africa-wide human-caused emission reductions could prevent about 96,000 and 84,000 $PM_{2.5}$-related deaths by 2050, though dust feedbacks may modify the magnitude of these health benefits.

1. Introduction

Emissions of anthropogenic aerosols and their precursors are projected to decline across most regions in the coming decades, driven by policies aimed at protecting human health from the adverse impacts of air pollution (Amooli et al., 2025; Lund et al., 2019; Rao et al., 2017; van Vuuren et al., 2011; Westervelt et al., 2015). This global and regional reduction of anthropogenic aerosols is expected to influence both global and regional precipitation patterns and surface temperatures (Allen et al., 2020; Rotstayn et al., 2013; Samset et al., 2018, 2025; Scannell et al., 2019; Shindell et al., 2012; Shindell & Smith, 2019; Westervelt et al., 2017, 2018; Wu et al., 2013). While most scenarios project widespread declines, Shared Socioeconomic Pathway 3–7.0 (SSP3–7.0) exhibits an initial increase in emissions during the early 21st century, followed by a decline around mid-century (Wilcox et al., 2023). Aerosols influence precipitation through direct (modifying radiation) and indirect (altering cloud microphysics) effects (Myhre et al., 2013; Stier et al., 2024). They suppress rainfall by increasing cloud droplet numbers, producing smaller droplets, which delays coalescence (Albrecht, 1989). Conversely, reducing aerosols generally enhances precipitation by allowing more solar radiation to reach the surface and increasing autoconversion via the cloud lifetime effect (Albrecht, 1989; Ramanathan et al., 2001). Aerosol composition modulates these responses: sulfate, as a scattering agent, and some organic aerosols, efficiently act as cloud condensation nuclei (CCN), whereas black carbon, an absorbing aerosol, seeds clouds less effectively (Bond et al., 2013; Ming et al., 2010; Westervelt et al., 2018). In parallel, mineral dust is a highly efficient ice-nucleating particle, especially due to feldspar-bearing fractions, although current Earth system models represent dust–ice interactions only crudely or omit them entirely (Atkinson et al., 2013; Kok et al., 2023). Some regions have already experienced substantial anthropogenic aerosol reductions in the past decades, whereas others are projected to undergo similar reductions in the near future (Bauer et al., 2022). In addition, aerosols reduce surface wind speeds by increasing boundary-layer stability, suppressing turbulence, and limiting downward momentum transfer (Jacobson & Kaufman, 2006; Miller, Tegen, & Perlwitz, 2004). Removing them reverses these effects, restoring downward mixing and strengthening near-surface winds, all of which are expected to reduce surface concentrations of pollutants (Li et al., 2024; Stjern et al., 2023).

While some of these previous studies include Africa as part of broader analyses, they have primarily examined African climate responses to global and regional anthropogenic aerosol reductions, with relatively little attention given to air quality impacts and the feedbacks between climate and air quality as modulated by Saharan dust. For example, Westervelt et al. (2017, 2018) showed that removing anthropogenic aerosols and precursors such as sulfur dioxide (SO_2), black carbon (BC), and organic aerosol (OA) in the United States, Europe, and China leads to increased warming in the Northern Hemisphere. This warming shifts the Intertropical Convergence Zone (ITCZ) northward, resulting in additional wet-season rainfall over the Sahel. Similarly, Scannell et al. (2019) and Navarro et al. (2017) reported that decreases in SO_2 emissions across the Northern Hemisphere midlatitudes cause a northward ITCZ shift and increase precipitation in the Sahel. More recently, Shindell et al. (2023) estimated that reduced African cooling aerosols account for about 33%–90% of the precipitation increase in a lower greenhouse gas (GHG) and aerosol emission pathway compared to business-as-usual over tropical Northern Hemisphere Africa during local summer. It is important to note that GHG-induced warming also affects the ITCZ position (Liu et al., 2024), which can modulate or complicate the aerosol-driven precipitation response.

Despite these advances, there is still limited understanding of how global and regional anthropogenic aerosol emission reductions will influence air quality in Africa, especially considering how the resulting changes in key meteorological drivers of dust may feed back on dust emissions and removal in the region, which is the largest dust source in the world and a major driver of African climate and air quality (Bauer et al., 2019; Evan et al., 2009; Huneeus et al., 2011; Kok et al., 2018). To address this knowledge gap, we analyze meteorological responses to the removal of anthropogenic aerosols from four world regions as well as globally, using simulations from eight fully coupled Earth system models participating in the Regional Aerosol Model Intercomparison Project (RAMIP) (Wilcox et al., 2023). This approach allows us to investigate changes in African air quality and the

James Keeble, Tsuyoshi Koshiro, Paul Kushner, Anna Lewinschal, Marianne T. Lund, Molly MacRae, Risto Makkonen, Joonas Merikanto, Larissa Nazarenko, Pierre Nabat, Declan O'Donnell, Naga Oshima, Geeta Persad, Steven T. Rumbold, Knut von Salzen, Bjørn H. Samset, Neil C. Swart, Toshihiko Takemura, Laura J. Wilcox, Daniel M. Westervelt

meteorological feedbacks on dust emissions in Africa in a more robust way than previous single-model studies (Aboagye-Okyere et al., 2025; Amooli et al., 2025; Bauer et al., 2019; Chowdhury et al., 2020; Wells et al., 2024).

Dust emissions are strongly modulated by meteorological conditions such as precipitation, surface wind speed and gustiness, and soil moisture, which control the availability and mobilization of erodible material (Cakmur et al., 2006; Ginoux et al., 2001; Kim et al., 2017; Knippertz & Todd, 2012; Miller et al., 2006; Pu & Ginoux, 2017, 2018). Warming from greenhouse gases is expected to increase dust loading over the Sahara, driven by stronger winds, resulting from changes in the land-sea temperature contrast combined with more frequent droughts (Clifford, 2019; Gomez et al., 2023; Jenkins et al., 2025). Changes in the meteorological drivers of dust emissions due to global and regional anthropogenic aerosol emission perturbations could further alter dust loading over Africa. However, the extent to which these feedbacks will amplify or counteract projected air quality improvements in Africa remains poorly understood.

Our study goes beyond existing literature by isolating the aerosol driven climate impact on dust emissions. Aerosols can influence dust emission processes through radiative and boundary-layer interactions (Engelstaedter et al., 2006; Miller, Perlwitz, & Tegen, 2004; Zender & Kwon, 2005). These aerosol–dust couplings provide an important pathway through which emission changes may influence regional dust responses and are discussed further in Section 3.2. Understanding dust aerosols is critical because they influence key Earth system processes, affecting the Earth's radiation budget, heterogeneous chemistry, cloud microphysics, and air quality, with implications for human health (Brey et al., 2020; Fan et al., 2014; Kok et al., 2023; Miller & Tegen, 1998; Miller, Tegen, & Perlwitz, 2004; Proestakis et al., 2025; Rosenfeld et al., 2001; Zhang et al., 2021). Dust emissions have increased by roughly 50%–55% since the mid-19th century, primarily driven by anthropogenic land-use changes, including agricultural expansion and drying of inland water bodies, with climate variability modulating regional trends (Kok et al., 2023; Leung et al., 2025). North African dust mass loading increased by ∼46% between the pre-industrial and modern periods, slightly below the global mean increase (∼55%) (Kok et al., 2023). Dust emissions are projected to either continue increasing or remain near present-day levels depending on future climate and land-use scenarios (Kok et al., 2023; Leung et al., 2025). Arid regions of Africa alone are estimated to emit roughly 800 Tg of soil dust annually, representing about 70% of global emissions and nearly six times greater than those from Asia, the second-largest source region (Adebiyi & Kok, 2020; Huneeus et al., 2011; Kok et al., 2021; Textor et al., 2006; Wu et al., 2020). Once airborne, dust can influence large-scale climate processes, such as Atlantic hurricane formation (Carlson & Prospero, 1972; Zhu et al., 2024), and becomes a significant component of fine particulate matter ($PM_{2.5}$) pollution, affecting air quality in downwind population centers (Amooli et al., 2024; Brey et al., 2020; Grineski et al., 2011; Westervelt et al., 2025).

Prolonged exposure to ambient $PM_{2.5}$ has been linked to numerous adverse health effects, including increased mortality from cardiovascular and cerebrovascular diseases, acute lower respiratory infections, lung cancer, and adverse birth outcomes (Burnett et al., 2018; Chowdhury et al., 2020, 2022; Cohen et al., 2017; Lelieveld et al., 2019; Li et al., 2018; Mallone et al., 2011; Murray et al., 2020; Pérez García-Pando et al., 2014; Pope et al., 2002). Ischemic heart disease (IHD) and stroke are major contributors to the health burden from air pollution (Fang et al., 2025), and the full range of $PM_{2.5}$-related conditions collectively contributes to a substantial global toll. Recent estimates attribute approximately 8.1 million deaths per year worldwide to $PM_{2.5}$ exposure (GBD, 2024).

In Africa, $PM_{2.5}$-related mortality has been increasing over the past decade (Amooli et al., 2025; Murray et al., 2020). While reductions in global and regional anthropogenic aerosol emissions are expected to improve air quality and reduce mortality, changes in meteorology-driven dust emissions could offset some of these benefits. Understanding this trade-off requires better knowledge of how dust contributes to the overall $PM_{2.5}$ health burden. Estimates of dust-related excess mortality as a share of global air pollution deaths vary widely, ranging from approximately 18%–33% of global $PM_{2.5}$-attributable deaths, with particularly high contributions (up to 50%) in the dust belt region (Evans et al., 2013; Giannadaki et al., 2014; Lim et al., 2012; McDuffie et al., 2021; Weagle et al., 2018). Some studies explored sensitivity assumptions in which anthropogenic $PM_{2.5}$ is treated as more toxic than mineral dust (Chowdhury et al., 2022; Lelieveld et al., 2015), whereas other studies assume equal toxicity across $PM_{2.5}$ components due to insufficient epidemiological evidence to distinguish health effects by source (Bauer et al., 2019; Stafoggia et al., 2013; Yang et al., 2022).

The structure of the paper is as follows. Section 2 describes the methodology, including details of the RAMIP simulations and participating models, the approach for calculating $PM_{2.5}$ concentrations, the assessment of

meteorological feedbacks on dust emissions, and the health impact analysis of anthropogenic aerosol emission perturbations relative to baseline simulations. Section 3 presents the results and discussion, including air quality changes, meteorological responses and their feedback on dust emissions, and the associated mortality impacts. Our conclusions are in Section 4.

2. Methods

2.1. Simulations and Models

This study uses simulations from RAMIP (Wilcox et al., 2023), which is part of the extended CMIP6 framework (CMIP6Plus). RAMIP builds upon and extends the historical simulations (1850–2014) provided to CMIP6 (Eyring et al., 2016), and all experiments are conducted within the framework of the SSPs (Riahi et al., 2017). RAMIP uses SSP3-7.0, characterized by weak air quality policies and sustained high aerosol emissions, as the baseline scenario. Regional perturbations of SO_2, BC, and organic carbon (OC) emissions are applied following the stronger air quality policy scenario SSP1-2.6 globally, and targeting individual emission regions including Africa and the Middle East (AFR), East Asia (EAS), North America and Europe (NAE), and South Asia (SAS), thereby isolating global, regional, and local climate and air quality responses to emissions changes in specific regions.

For this study, we analyzed the RAMIP AFR (SSP370-afr126aer), EAS (SSP370-eas126aer), NAE (SSP370-nae126aer), SAS (SSP370-sas126aer), and global (SSP370-126aer) simulations, where anthropogenic aerosol emissions within defined geographical boxes encompassing these regions are perturbed (SSP3-7.0 replaced with SSP1-2.6), as defined in Wilcox et al. (2023). We assessed the influence of these regional perturbations on African air quality, with a particular focus on direct changes from anthropogenic emissions reductions and indirectly through meteorological feedbacks affecting dust emissions. Emissions over Africa continue to increase in SSP3-7.0 (Amooli et al., 2025; Wilcox et al., 2023), though the growth in the difference between SSP3-7.0 and SSP1-2.6 slows in the second half of the century (Wilcox et al., 2023). During the 2030–2049 period analyzed in our study, SSP3-7.0 exceeds SSP1-2.6 by roughly 8%–23% (derived from Wilcox et al., 2023; Figure 2). All participating models conducted both baseline and perturbed simulations for the period 2015–2051, providing 10 ensemble members per simulation. Each ensemble member was initialized with slightly different atmospheric initial conditions, as further described by Wilcox et al. (2023). This approach allows us to quantify internal climate variability and isolate the forced response to anthropogenic aerosol perturbations. We used outputs from eight Earth System Models participating in RAMIP, each run in a fully coupled atmosphere–ocean mode comprising an 80-member multi-model ensemble. Model outputs were retained on their native grids except when calculating the multi-model mean (MMM), for which all outputs were regridded to the horizontal resolution of the UKESM1-0-LL model (1.25° × 1.875°), chosen because UKESM1-0-LL represents an intermediate resolution among the participating models (Table 1). A summary of the RAMIP participating models and simulations used in this study is presented in Tables 1 and 2. Further technical details of the models and configurations of RAMIP are provided in Samset et al. (2025) and Wilcox et al. (2023).

Hereafter, we refer to these models (Table 1) by their short names: GISS, CESM, EC-Earth, NorESM, MRI, CNRM, CanESM, and UKESM.

Climate and air quality responses over Africa are quantified as the differences between each regional perturbation scenario (SSP370-126aer, SSP370-afr126aer, SSP370-eas126aer, SSP370-nae126aer, and SSP370-sas126aer) and the baseline (SSP3-7.0), averaged annually across all years and ensemble members over the period 2030–2049, with additional analyses of seasonal changes in dust emissions and precipitation. Africa is defined here as a geographical domain spanning 40°S–40°N and 25°W–52°E. Our domain differs slightly from the RAMIP "Africa" perturbation region (35°S–35°N, 20°W–60°E), as it extends further north and south and is shifted westward to focus specifically on the African continent and its major dust source regions, while excluding parts of the Middle East.

2.2. $PM_{2.5}$ Calculation Approaches

Of the eight RAMIP models analyzed, five provided explicit size outputs of $PM_{2.5}$ (Table 1), while the others provided either bulk aerosol concentrations or individual aerosol components without necessarily an explicit $PM_{2.5}$ diagnostic, thereby requiring an estimate of the $PM_{2.5}$ fraction adopted by Turnock et al. (2020;

Table 1
RAMIP Participating Models Used in This Analysis and Their Key References

Model	Resolution (lat × lon)	$PM_{2.5}$ diagnostic	Dust emission scheme	Model description paper
GISS-E2-1-G	2° × 2.5°	Yes	(Cakmur et al., 2006; Miller et al., 2006)	(Bauer et al., 2020; Kelley et al., 2020)
CESM2	0.9° × 1.25°	Yes	Zender et al. (2003)	Danabasoglu et al. (2020)
EC-Earth3-AerChem	0.7° × 0.7°	Yes	van Noije et al. (2021)	van Noije et al. (2021)
NorESM2-LM	1.875° × 2.5°	Yes	Zender et al. (2003)	Seland et al. (2020)
MRI-ESM2-0	1.125° × 1.125°	Yes	Tanaka and Chiba (2005)	Yukimoto et al. (2019)
CNRM-ESM2-1	1.4° × 1.41°	No	(Kok, 2011; Marticorena & Bergametti, 1995)	Séférian et al. (2019)
CanESM5-1	2.80° × 2.80°	No	Marticorena and Bergametti (1995)	Swart et al. (2019)
UKESM1-0-LL	1.25° × 1.875°	No	Woodward (2001)	Sellar et al. (2019)

Note. All models include interactive dust emission modules.

Equation 1). For the five models with explicit PM2.5 diagnostics, we compared each model's explicit $PM_{2.5}$ direct output with the approximated $PM_{2.5}$ estimate derived using the CMIP6 10% dust fraction approximation (Turnock et al., 2020) to assess the accuracy of this approximate method commonly used in CMIP6-based analyses.

$$\text{CMIP6 Approx. } PM_{2.5} = BC + SO_4 + OA + (0.25 \times SS) + (0.1 \times DU) \quad (1)$$

where BC is black carbon, SO_4 is sulfate, OA is organic aerosol, SS is sea salt, and DU is the total dust mass.

In models with size-resolved aerosol schemes, $PM_{2.5}$ is computed as the sum of at least BC, sulfate (SO_4), OA, dust $PM_{2.5}$, and sea salt $PM_{2.5}$ (Ran et al., 2023), with some models such as GISS including ammonium and nitrate (Bauer et al., 2007). The size-integrated dust and sea salt components are computed by summing the mass in the fine aerosol modes (e.g., Aitken and accumulation) along with a model-specific fraction of the coarse-mode mass that falls below the 2.5 μm aerodynamic diameter threshold, typically determined from a lognormal size distribution in modal approaches or by summing bins in sectional schemes. These components were provided directly by the models and reflect each model's internal size definitions and assumptions. Size-resolved dust $PM_{2.5}$ components were available in GISS and CESM. In CESM, dust $PM_{2.5}$ is computed as:

$$\text{Exact Dust } PM_{2.5} = DU_{a1} + DU_{a2} + 0.136 \times DU_{a3} \quad (2)$$

where DU_{a1} and DU_{a2} represent the accumulation and Aitken modes, and DU_{a3} is the coarse mode.

In the GISS model, which uses a sectional scheme, dust $PM_{2.5}$ is computed using:

$$\text{Exact Dust } PM_{2.5} = \text{Clay} + 0.322 \times \text{Silt1} \quad (3)$$

where clays are modeled as ranging from 0.2 to 2 μm in diameter and Silt1 from 2 to 4 μm (Perlwitz et al., 2015). Note that for dust, $PM_{2.5}$ in the models is based on geometric diameter rather than strict aerodynamic diameter. Because dust particles are non-spherical and have varying density, the 2.5 μm aerodynamic diameter corresponds

Table 2
RAMIP Simulations Used in This Analysis

RAMIP simulation name	Aerosol emissions	Ensemble members
SSP370-126aer (Global)	SSP1-2.6	10
SSP370-afr126aer (AFR)	SSP1-2.6 within the Africa and Middle East region, SSP3-7.0 elsewhere	10
SSP370-eas126aer (EAS)	SSP1-2.6 within the East Asia region, SSP3-7.0 elsewhere	10
SSP370-nae126aer (NAE)	SSP1-2.6 within the North America and Europe regions, SSP3-7.0 elsewhere	10
SSP370-sas126aer (SAS)	SSP1-2.6 within the South Asia region, SSP3-7.0 elsewhere	10

Note. All simulations use SSP3-7.0 as the baseline scenario.

roughly to 2 μm geometric diameter (Yang et al., 2022). This may introduce a small bias relative to standard health exposure metrics. The differences in coarse-mode contributions to dust $PM_{2.5}$ reflect variations in the bin- and modal-based aerosol size representations across models. While most models apply similar size-resolved approaches, the specific fraction of coarse-mode dust included varies and is not always explicitly documented.

In the absence of an explicitly provided size-dependent output for dust, the CMIP6 approximation follows Equation 1 for total $PM_{2.5}$ (Turnock et al., 2020) and the final term of Equation 1 for dust-specific $PM_{2.5}$. The comparison to explicit dust size-distributions in the GISS and CESM models is used to evaluate the potential bias introduced by the 10% dust fraction assumption across models.

2.3. Assessment of the Meteorological Feedback on Dust Emissions in GISS

To assess the meteorological feedbacks driving dust emission changes resulting from anthropogenic aerosol reductions, we performed the analysis using the GISS model, which has a sophisticated representation of the dust cycle, including a subgrid wind parameterization and identification of major dust-emitting regions (Cakmur et al., 2006; Miller et al., 2006). These improvements lead to more realistic emission, transport, and deposition processes as well as enhanced meteorological interactivity compared to a model without preferred sources and emission dependence upon gustiness (Cakmur et al., 2006; Miller et al., 2006). Fire emissions, just like anthropogenic emissions, are treated as prescribed inputs and do not respond to meteorology, while sea salt and dimethyl sulfide (DMS) emissions respond to meteorology but are primarily located over the Southern Ocean, and thus have minimal influence on $PM_{2.5}$ over Africa. Consequently, this analysis focuses on meteorological controls on dust emission changes. We conducted multiple linear regressions (ordinary least squares) between changes in dust emissions and changes in four key meteorological drivers at the annual scale for the period 2030–2049, following Equation 4 (Aryal & Evans, 2023; Pu & Ginoux, 2018; Zhao et al., 2022).

$$\text{Dust} = \beta_0 + \beta_W.W^3 + \beta_P.P + \beta_T.T + \beta_C.C + \varepsilon \tag{4}$$

where Dust is the dust emission time series at a grid point (kt yr^{-1}), W is the surface total wind speed time series at a grid point (m s^{-1}), derived from the individual components of the zonal (u) and meridional (v) winds:

$$W = \sqrt{u^2 + v^2} \tag{5}$$

P is the precipitation time series at a grid point (mm day^{-1}), T is the threshold velocity for dust emissions, parameterized as a function of soil moisture (Miller et al., 2006) time series at a grid point (m s^{-1}), C is the dry convective velocity scale (related to wind gustiness) time series at a grid point (m s^{-1}), β_0 is the intercept, β_W, β_P, β_T, and β_C are the regression coefficients of the meteorological variables, and ε is the error term.

We used the cube of near-surface wind speed as a predictor because dust emission flux scales with the third power of wind speed (Evans et al., 2016; Kim et al., 2013). For GISS, CESM, EC-Earth, NorESM, MRI, and CanESM, we used the mean of the cubed wind speed at each time step. In CNRM and UKESM, where daily time steps were not available, we used the cube of the monthly mean 10 m wind speed; we note that this approach may underestimate the contribution of high-wind events. These variables were selected because they are directly linked to dust emissions in the GISS model, noting that the meteorological drivers and their implementation vary across models. All time series represent changes relative to the baseline due to anthropogenic aerosol reductions. We normalized both the dust emission and meteorological driver time series by their standard deviation before performing the regression, allowing the resulting coefficients to be compared directly across predictors since they are expressed on the same scale.

To assess the performance of the regression model, we calculated the Pearson correlation coefficient (r) and the coefficient of determination (R^2). We also computed the normalized root mean squared error (nRMSE):

$$\text{nRMSE} = \frac{\text{RMSE}}{\sum y} \times 100 \tag{6}$$

where

$$\mathrm{RMSE} = \sqrt{\frac{1}{n}\sum (y - \hat{y})^2} \tag{7}$$

and coefficient of variation of the mean absolute error (CvMAE):

$$\mathrm{CvMAE} = \frac{\mathrm{MAE}}{\sum y} \times 100 \tag{8}$$

where

$$\mathrm{MAE} = \frac{1}{n}\sum |y - \hat{y}| \tag{9}$$

Both nRMSE and CvMAE are normalized by the sum of dust emission values at each grid cell (Giordano et al., 2021). Here, $\hat{y}$ are the predicted values from the regression model and y are the time series values of the meteorological variable and/or dust emissions.

2.4. Health Impact Assessment

To estimate total $PM_{2.5}$- and dust $PM_{2.5}$-attributable mortality in 2050, we applied the cause-specific Meta-Regression-Bayesian, Regularized, Trimmed (MR-BRT) exposure-response function (Chowdhury et al., 2022; Murray et al., 2020; Pozzer et al., 2023) to year 2050 simulated $PM_{2.5}$ concentrations across the eight models. Mortality was assessed for six major diseases: IHD, stroke (both ischemic and hemorrhagic), chronic obstructive pulmonary disease (COPD), lung cancer (LC), and type II diabetes mellitus (T2DM) in adults aged 25 years and older, as well as acute lower respiratory tract infections (ALRI) in children under 5 years (Aboagye-Okyere et al., 2025; Amooli et al., 2025; Chowdhury et al., 2022, 2024; Lelieveld et al., 2015; Yang et al., 2022). Cause-specific relative risks (RRs) were obtained directly from Chowdhury et al. (2022), based on the MR-BRT function, and have also been used in recent studies (Amooli et al., 2025; Chowdhury et al., 2022, 2024). These RRs vary by disease, age group, and annual $PM_{2.5}$ concentration, with age-specific RRs provided for IHD and stroke, and uniform RRs applied for LC, T2DM, and COPD across all adult age groups. We assumed a theoretical minimum risk exposure level of 2.4 μg m^{-3}, the lower bound of the GBD-recommended range (2.4–5.9 μg m^{-3}), and held it constant across all locations and scenarios, below which no mortality is assumed (Chowdhury et al., 2022; Murray et al., 2020). This conservative choice ensures that mortality estimates capture the maximum attributable burden, while sensitivity tests indicate that relative differences across scenarios remain consistent in highly polluted regions (Chowdhury et al., 2022). To account for differences in model structure and capture inter-model ensemble uncertainty, $PM_{2.5}$-attributable mortality was calculated separately for each model using model-specific annual $PM_{2.5}$ concentrations. The resulting mortality estimates were then averaged to obtain the multi-model mean. Uncertainty in $PM_{2.5}$-attributable mortality was quantified by propagating the 95% confidence intervals (CI) of the RRs (Figure S1 in Supporting Information S1) through the health impact function and by incorporating the 95% spread of the inter-model ensemble.

Calculations were performed for the baseline SSP3-7.0 simulation and for regional perturbations following SSP1-2.6, holding the population and baseline mortality constant at SSP3 2050 levels to isolate mortality changes attributable to regional aerosol emission reductions. A 0.0083° × 0.0083° SSP3 population distribution for 2050 was obtained from the National Aeronautics and Space Administration (NASA) Socioeconomic Data and Applications Center (SEDAC) gridded population product (Jones et al., 2020) and aggregated to match the common analysis grid (1.25° × 1.875°), to which all model $PM_{2.5}$ and dust $PM_{2.5}$ fields were regridded prior to analysis. Using the gridded population data, we spatially distributed the age-specific SSP3 population projections for 2050 from the SSP database (KC et al., 2024; Riahi et al., 2017), which provide total population counts by age for each country at 5-year intervals, to obtain gridded age-specific population counts. These gridded age-specific populations were combined with SSP3 country-level baseline mortality rates (per 100,000 people) from the Global Burden of Disease (GBD) Foresight data set for 2050 (GBD, 2024), for each disease and age, to calculate baseline deaths per grid cell. Using the GBD Foresight data ensures consistency with the GBD baseline data commonly used in health assessments.

Finally, multiplying the baseline deaths by the attributable fraction (AF) for the corresponding disease and age yielded $PM_{2.5}$- and dust $PM_{2.5}$-attributable mortality estimates for each grid cell (Equation 10) (Amooli et al., 2025; Chowdhury et al., 2020; Southerland et al., 2022).

$$M_{d,a} = P_a \times \mathrm{BM}_{d,a} \times \mathrm{AF}_{d,a} \tag{10}$$

$M_{d,a}$ is the $PM_{2.5}$- or dust $PM_{2.5}$-attributable mortality in a grid cell by disease and age; $\mathrm{BM}_{d,a}$ is the baseline mortality rate per 100,000 population by disease and age; P_a is the exposed population in a grid by age; and $\mathrm{AF}_{d,a}$ is the attributable fraction by disease and age, calculated as:

$$\mathrm{AF}_{d,a} = \frac{\mathrm{RR}_{c,d,a} - 1}{\mathrm{RR}_{c,d,a}} \tag{11}$$

$\mathrm{RR}_{c,d,a}$ is the Relative Risk, where c,d,a denotes the model-specific annual $PM_{2.5}$ or dust $PM_{2.5}$ concentration in a grid, disease, and age, respectively. The attributable fraction represents the proportion of deaths in each grid cell that can be attributed to $PM_{2.5}$ or dust $PM_{2.5}$ exposure based on the relative increase in risk. For dust $PM_{2.5}$, we applied the same MR-BRT function as for total $PM_{2.5}$, assuming similar toxicity per unit mass, consistent with the MR-BRT formulation. Previous studies using the Integrated Exposure-Response (IER) function and the Global Exposure Mortality Model (GEMM) have also made identical assumptions (e.g., Aboagye-Okyere et al., 2025; Burnett et al., 2018; Im et al., 2023; Ostro et al., 2021; Southerland et al., 2022; Yang et al., 2022). Nevertheless, we note that natural dust could be less toxic in some contexts, which may lead to an overestimation of dust-attributable mortality in this study.

Cause-specific $PM_{2.5}$-attributable mortality estimates were computed by applying the full exposure-response function (MR-BRT; Chowdhury et al., 2022) separately to the model-specific $PM_{2.5}$ concentrations in each scenario, including both the baseline and perturbed scenarios. Total $PM_{2.5}$-attributable mortality was obtained by summing across causes and age groups, and a similar approach was used to estimate total dust $PM_{2.5}$-attributable mortality. Avoided deaths from regional anthropogenic aerosol emission reductions were then calculated as the difference between the baseline scenario and the perturbed scenario:

$$\text{Avoided deaths} = \text{Mortality}_{\text{baseline}} - \text{Mortality}_{\text{regional perturbations}} \tag{12}$$

Because the exposure-response relationship is nonlinear, the health impact of a given change in $PM_{2.5}$ depends on the baseline concentration. This dependence is inherently captured by applying the full exposure-response function separately to each scenario's concentration field rather than concentration differences.

3. Results and Discussion

In this section, we first evaluate the method for estimating $PM_{2.5}$ that will be used in subsequent analyses. We then present $PM_{2.5}$ and dust emission responses to anthropogenic aerosol emission reductions, followed by the meteorological response to anthropogenic aerosol changes and feedbacks on dust emissions. Next, we perform a regression analysis using the GISS model to quantify the sensitivity and relative importance of meteorological drivers of dust emissions. Finally, we estimate excess mortality attributable to total $PM_{2.5}$ and dust $PM_{2.5}$ from the anthropogenic aerosol emission reductions.

We begin by providing a systematic multi-model assessment of the CMIP6 $PM_{2.5}$ approximation against the per model's aerosol microphysics-based $PM_{2.5}$ outputs. We find that the CMIP6 10% dust fraction approximation can introduce biases in the $PM_{2.5}$ response to anthropogenic aerosol emission reductions (Figures S2 and S3 in Supporting Information S1). The approximation tends to overestimate $PM_{2.5}$ concentrations near source regions and underestimate transported $PM_{2.5}$, although the magnitude and sign of this difference vary across models and there is no consistent Africa-wide agreement. This occurs likely because a larger fraction of dust mass near sources is coarse (Diameter >2.5 μm) compared to remote regions with mostly fine particles. These results are consistent with previous studies that showed that the approximation increases biases relative to observations (Allen et al., 2020; Fiore et al., 2012; Im et al., 2018; Tsigaridis et al., 2014; Turnock et al., 2020; Zhao et al., 2021). Given these findings, in subsequent analyses, we used size-resolved $PM_{2.5}$ outputs for the five

models that provided them (Table 1), and the CMIP6 approximation for the remaining three models in which the dust $PM_{2.5}$ variable was unavailable.

Previous evaluation of the CMIP6 models used in this study indicates that they generally capture the seasonal and annual $PM_{2.5}$ cycles well in Western Africa when compared with surface observations, although concentration magnitudes exhibit substantial inter-model diversity (Toolan, Amooli, et al., 2025). In contrast, model performance is weaker in Eastern Africa, where $PM_{2.5}$ levels are more strongly influenced by local emissions and regional meteorology, including the East African monsoon, which models simulate less accurately. These regional differences in present-day model performance provide context for interpreting the spread in projected $PM_{2.5}$ responses across models.

3.1. $PM_{2.5}$ and Dust Emission Responses to Anthropogenic Aerosol Changes

An overview of the MMM and individual model responses of total $PM_{2.5}$ and its components across the AFR, NAE, and Global perturbations is shown in Figure 1, which summarizes the magnitude of ensemble responses, the relative contributions of aerosol components, and associated uncertainties across models. For a future African and global reduction in anthropogenic aerosol emissions (the RAMIP AFR and Global perturbations), multi-model mean concentrations of $PM_{2.5}$ decline substantially over Africa, with continental-average reductions of 0.92 ± 0.17 μg m^{-3} (5%) and 1.35 ± 0.50 μg m^{-3} (7%), respectively (Figures 1a and 1c, leftmost bars). The uncertainties represent the standard deviation across all models from the MMM.

The spatial distribution of these changes is shown in the left column of Figure 2. Declines are pronounced in densely populated regions, including Nigeria, Ethiopia, and Uganda, where decreases reach up to 12 μg m^{-3} (19%). Among the non-local regional anthropogenic aerosol emissions perturbations, reductions in North America and Europe (NAE) emissions are the only ones that improve African air quality, resulting in a continental-mean decrease of 0.29 ± 0.32 μg m^{-3} (2%; Figure 1b, leftmost bar). However, the inter-model spread exceeds the MMM response, indicating that these improvements are not statistically robust across models. The spread in NAE emissions reductions likely arises from differences in how individual models simulate the relevant teleconnections and Sahel precipitation responses, which in turn affect African $PM_{2.5}$ reductions. These improvements arise from remote teleconnections: anomalous Northern Hemisphere warming alters the intensity and location of the ITCZ, enhancing Sahel precipitation (Guo et al., 2024; Hirasawa et al., 2022; Monerie et al., 2023; Toolan, Amooli, et al., 2025; Undorf et al., 2018; Westervelt et al., 2017, 2018), which in turn reduces $PM_{2.5}$ through wet deposition and by limiting dust emissions from the surface (Aryal & Evans, 2023; Toolan et al., 2024; Westervelt et al., 2016). In addition, long-range transport of aerosols, particularly from Europe, plays a role in Northern Africa air quality. This transported aerosol is an important part of the mechanism for African precipitation responses to European aerosol perturbations (Dong et al., 2014). There is considerable model disagreement regarding the direction of African $PM_{2.5}$ changes resulting from anthropogenic aerosol emission reductions in South and East Asia (Figure S4 in Supporting Information S1). Furthermore, the direct influence of anthropogenic aerosol emission reductions in South and East Asia on African anthropogenic $PM_{2.5}$ through long-range transport is small (Figures S5–S7 in Supporting Information S1). Consequently, South and East Asia were excluded from the main analysis.

The multi-model mean $PM_{2.5}$ reductions are consistent with the multi-model mean reductions in the surface concentrations of BC, SO_4, and OA (Figures 1d–1l, leftmost bars). On a continental-average, BC, SO_4, and OA decrease by 0.16 ± 0.03 μg m^{-3} (46%), 0.25 ± 0.09 μg m^{-3} (19%), and 0.57 ± 0.10 μg m^{-3} (25%) under the AFR perturbations, and by 0.18 ± 0.04 μg m^{-3} (51%), 0.43 ± 0.15 μg m^{-3} (33%), and 0.64 ± 0.11 μg m^{-3} (28%) under the Global perturbations. The spatial distribution of these reductions is shown in Figure 3 (individual model results are provided in Figures S5–S7 of Supporting Information S1). The strongest declines, up to 6 μg m^{-3}, occur over Nigeria, Uganda, Ethiopia, and parts of northern Africa, particularly the Mediterranean region. These changes are consistent with expectations for RAMIP given the emission perturbations applied in the experiment. However, while reductions in anthropogenic aerosols are substantial, the total $PM_{2.5}$ response is moderated by dust, which partially offsets these decreases. This highlights that the response to anthropogenic emission reductions is relatively straightforward, but the total $PM_{2.5}$ signal is complicated by the natural dust contribution. Additionally, SO_4 and OA remain elevated by up to 1.5 μg m^{-3} over Angola and Zambia where biomass burning aerosols are higher under SSP1 than under SSP3 (Amooli et al., 2025). The results demonstrate that local and global anthropogenic aerosol emission reductions primarily affect regions close to major anthropogenic sources,

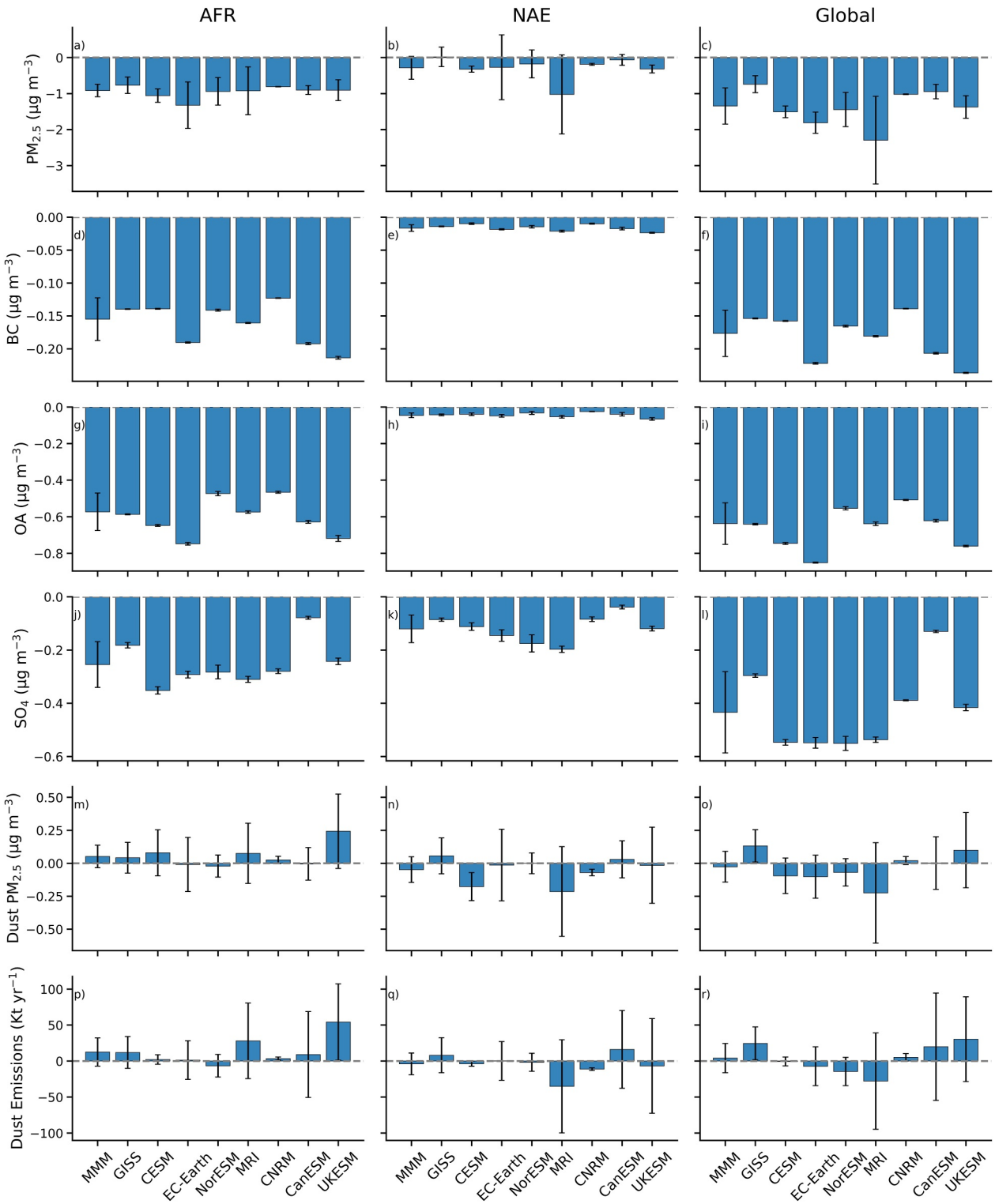

Figure 1. Aggregated summary of MMM and individual model aerosol responses across regional perturbation experiments. Bar charts show the MMM (leftmost bar in each panel) and individual model responses for total $PM_{2.5}$ (a–c) and its components: BC (d–f), OA (g–i), SO_4 (j–l), and dust $PM_{2.5}$ (m–o), and dust emissions (p–r), across AFR (first column), NAE (second column), and Global perturbations (third column). Error bars denote the inter-model standard deviation for the MMM and the intra-ensemble member uncertainty for individual models. Averages are computed over the analysis domain defined in Figure 2.

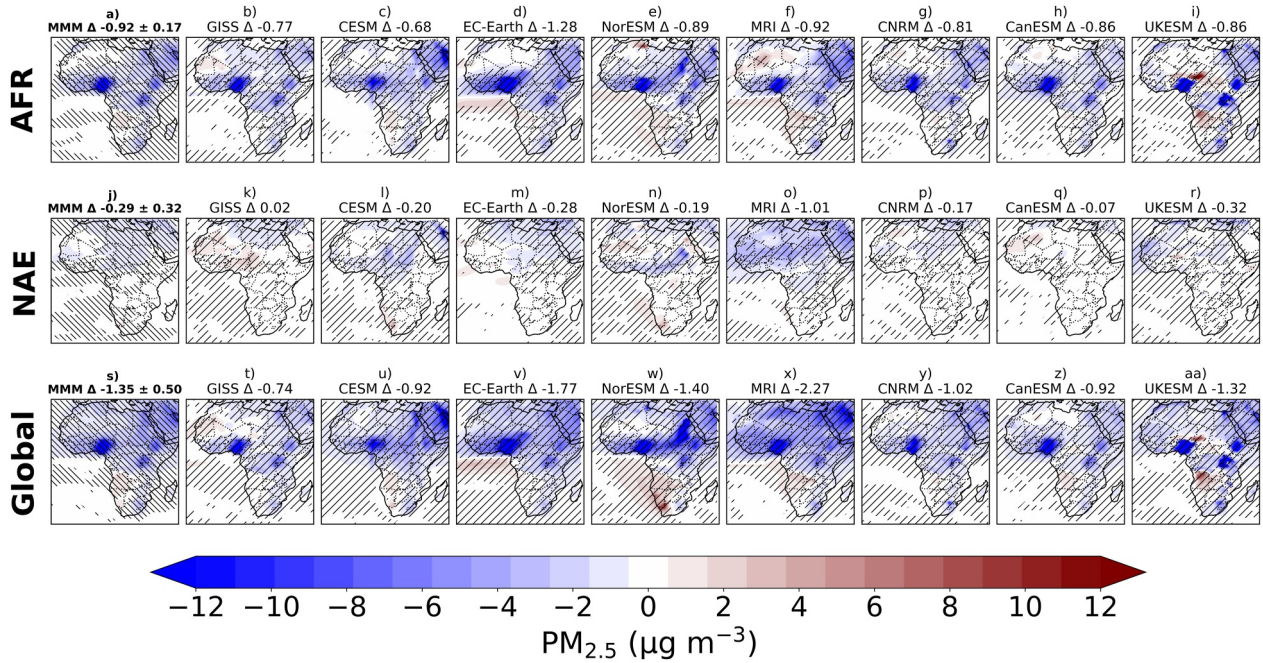

Figure 2. Annual mean $PM_{2.5}$ changes for the period 2030–2049, shown as differences between each regional perturbation simulation and the baseline simulation. Numbers at the top of each subplot indicate average annual $PM_{2.5}$ changes over Africa. Hatching in MMM (left column) indicates regions where ≥70% of models agree on the sign of the change. Hatching in the individual model panels indicates regions where ≥70% of ensemble members agree on the sign of the change. The plotted domain corresponds to 40°S–40°N and 25°W–52°E and is used consistently across all figures unless otherwise specified.

whereas the influence of remote regions is spatially heterogeneous and weaker, consistent with broader assessments of regional aerosol perturbation experiments (Chou et al., 2005; Persad & Caldeira, 2018; Westervelt et al., 2018).

Continental dust $PM_{2.5}$ responses are small compared to their uncertainty, with MMM changes of 0.05 ± 0.09 μg m^{-3} (0.8%) under AFR perturbations, -0.05 ± 0.10 μg m^{-3} (−0.8%) and -0.03 ± 0.12 μg m^{-3} (−0.5%) under NAE and Global perturbations, respectively (Figures 1m–1o, leftmost bars). Continent-wide averages are small in part due to opposite-signed signals in continental sub-regions. However, clearer responses emerge in regional averages of major dust source regions, such as the Bodélé Depression in northern Chad, a region known for its high dust emissions (Ali et al., 2022), and the Namib desert (Figure 4, left column). In Chad, the MMM indicates a robust decrease in dust $PM_{2.5}$ under the NAE perturbation (0.31 ± 0.17 μg m^{-3}; 1.2%), while the Namib desert shows a robust increase under the Global perturbation (0.18 ± 0.16 μg m^{-3}; 4.6%). Under the AFR perturbation, dust $PM_{2.5}$ increases are visible over northern Chad; however, the regionally averaged response (0.35 ± 0.44 μg m^{-3}; 1.4%) is not robust across the ensemble.

These changes in dust $PM_{2.5}$ are driven by changes in dust emissions (Figure 5, left column). Emission responses are most evident in major dust source regions, particularly in northern Chad and the Namib desert. In Chad, dust emissions show positive mean changes under the AFR perturbation (146.25 ± 211.98 kt yr^{-1}; 3.9%) and the Global perturbation (103.20 ± 165.09 kt yr^{-1}; 2.8%), whereas the NAE perturbation shows a negative mean change (-20.94 ± 59.74 kt yr^{-1}; −0.6%). In the Namib desert, dust emission changes are smaller but show positive responses under all perturbations. However, all regional-mean responses exhibit substantial inter-model spread and are not robust across the ensemble. While dust emissions are concentrated in key source regions such as Chad in the Sahara and Namib deserts, long-range transport spreads dust widely, influencing $PM_{2.5}$ in downwind regions (Evan et al., 2016; Knippertz & Todd, 2012; Prospero, 1999). Continental-average dust emissions show relatively small mean changes relative to inter-model uncertainty, with no robust ensemble-wide signal under any perturbation: 12.69 ± 20 kt yr^{-1} (1.2%) under AFR, 4.09 ± 20 kt yr^{-1} (0.4%) under Global, and -3.97 ± 15 kt yr^{-1} (−0.4%) under NAE anthropogenic aerosol emission reductions (Figures 1p–1r, leftmost bars). The large inter-model spread indicates that these mean changes are not statistically distinguishable from zero. Nevertheless, the sign and magnitude of the mean responses suggest potential mechanistic differences

across scenarios: dust emissions may influence the net $PM_{2.5}$ response in some cases, but these effects are small relative to model uncertainty and are not robust across the ensemble. On a continental mean, dust $PM_{2.5}$ changes account for approximately 14% of total $PM_{2.5}$ changes under AFR perturbations, 19% under NAE, and 11% under Global perturbations; however, these contributions are not robust across the ensemble (Figure S8 in Supporting Information S1). Regionally, dust $PM_{2.5}$ changes contribute up to 70% of total $PM_{2.5}$ changes over the Sahara and Namib deserts, but offset as much as 20% of reductions over Western and Eastern Africa and parts of the Mediterranean. In the baseline simulation, dust $PM_{2.5}$ contributes up to 50% of total $PM_{2.5}$ in the deserts (Figure S8 in Supporting Information S1). Despite these regional contributions, the projected scenario-driven changes in atmospheric dust loading over North Africa during our study period (−2 to +4%) are substantially smaller than the 46% historical increase reported by Kok et al. (2023), which examined past land-use and climate changes. This suggests that long-term land-use and climate changes exert a stronger control on dust loading than the mid-21st-century aerosol pathway differences examined here.

We now examine individual model responses of total $PM_{2.5}$, dust $PM_{2.5}$, and dust emissions across all perturbations. Inter-model variability in magnitude is summarized in Figure 1, while the corresponding spatial patterns are shown in Figures 2, 4, and 5. Spatially, several models (GISS, CESM, EC-Earth, CNRM, and CanESM) broadly reproduce the regionally mixed MMM patterns across all variables and perturbations. In contrast, MRI consistently departs from the MMM under NAE and Global perturbations, producing substantial and more spatially extensive anomalies. NorESM and UKESM also exhibit localized departures, showing positive dust responses under AFR and Global perturbations that are absent in the MMM. Beyond deviations from the MMM, there is substantial inter-model variability in the magnitude and spatial distribution of total $PM_{2.5}$ changes, dust $PM_{2.5}$ changes and dust emissions changes across models. To further examine how these differences appear in the key dust source regions highlighted in the MMM analysis, we focus on Chad and the Namib desert. For instance, NorESM shows $PM_{2.5}$ increases of up to 10 μg m^{-3} in the Namib Desert (Figure 2w), driven by enhanced dust $PM_{2.5}$ from local feedbacks on dust emissions (Figures 4 and 5) under the Global anthropogenic aerosol reductions simulation, whereas CESM and CNRM do not show any increase. Similarly, UKESM under AFR and Global anthropogenic aerosol reductions projects $PM_{2.5}$ increases of up to 12 μg m^{-3} in the Bodélé Depression, Angola, and Zambia (Figures 2i and 2aa), whereas the other models do not simulate $PM_{2.5}$ increases of this magnitude. These increases partly reflect contributions from anthropogenic aerosol components, including OA from residential fuel use in Angola and SO_4 from industrial coal combustion in Zambia (Figures S5–S7 in Supporting Information S1). Because anthropogenic emissions are prescribed and identical across models, the resulting anthropogenic aerosol responses tend to show smaller inter-model spread and are largely emissions-driven, reflecting the stronger and imposed nature of the anthropogenic signal. Nevertheless, some variability remains in the magnitude of SO_4 and OA responses due to differences in model chemistry, transport, and aerosol processes. This pattern is consistent with findings reported in Amooli et al. (2025) for SSP1, where anthropogenic emissions in Angola and Zambia were higher than in SSP3. In contrast, enhanced dust emissions from the Bodélé and Namib source regions further contribute to the $PM_{2.5}$ increases through the corresponding increases in dust $PM_{2.5}$. Unlike anthropogenic aerosols, dust emissions are process-driven and depend strongly on the representation of surface winds, soil properties, and emission parameterizations, leading to larger inter-model variability (Kok et al., 2023; Miller et al., 2006; Pu & Ginoux, 2017). Although finer resolution and more advanced physics have improved the ability of climate models to simulate dust processes from the mesoscale to the global scale, substantial uncertainties remain (Adebiyi & Kok, 2020; Kok et al., 2017; Zhao et al., 2022). Incomplete representation of the meteorological drivers of dust emission, transport and deposition, combined with uncertainties in dust particle size, shape and model structure (Adebiyi & Kok, 2020; Evan, 2018; Wu et al., 2020; Zhao et al., 2022), contribute directly to the large inter-model spread in response magnitude (Figure 1) and in the spatial patterns of dust concentrations (Figure 4) and dust emissions (Figure 5). Some models (CESM and NorESM) exhibit comparatively limited dust emission variability in certain regions (Figure 5), which contributes to their smaller response magnitudes relative to other models. These differences reflect model-specific dust source representation and emission parameterizations and contribute to the overall inter-model spread.

While the spatial analysis highlights responses in key dust source regions such as Chad and the Namib Desert, continental-average changes provide a broader perspective on how dust emissions influence the total $PM_{2.5}$ signal across models. At the continental scale, dust $PM_{2.5}$ changes arising from dust emission responses modify the total $PM_{2.5}$ changes in individual models, sometimes substantially, but anthropogenic aerosol changes remain the primary driver of the overall $PM_{2.5}$ response. The largest absolute decreases in dust emissions (7.11 Kt yr^{-1} in

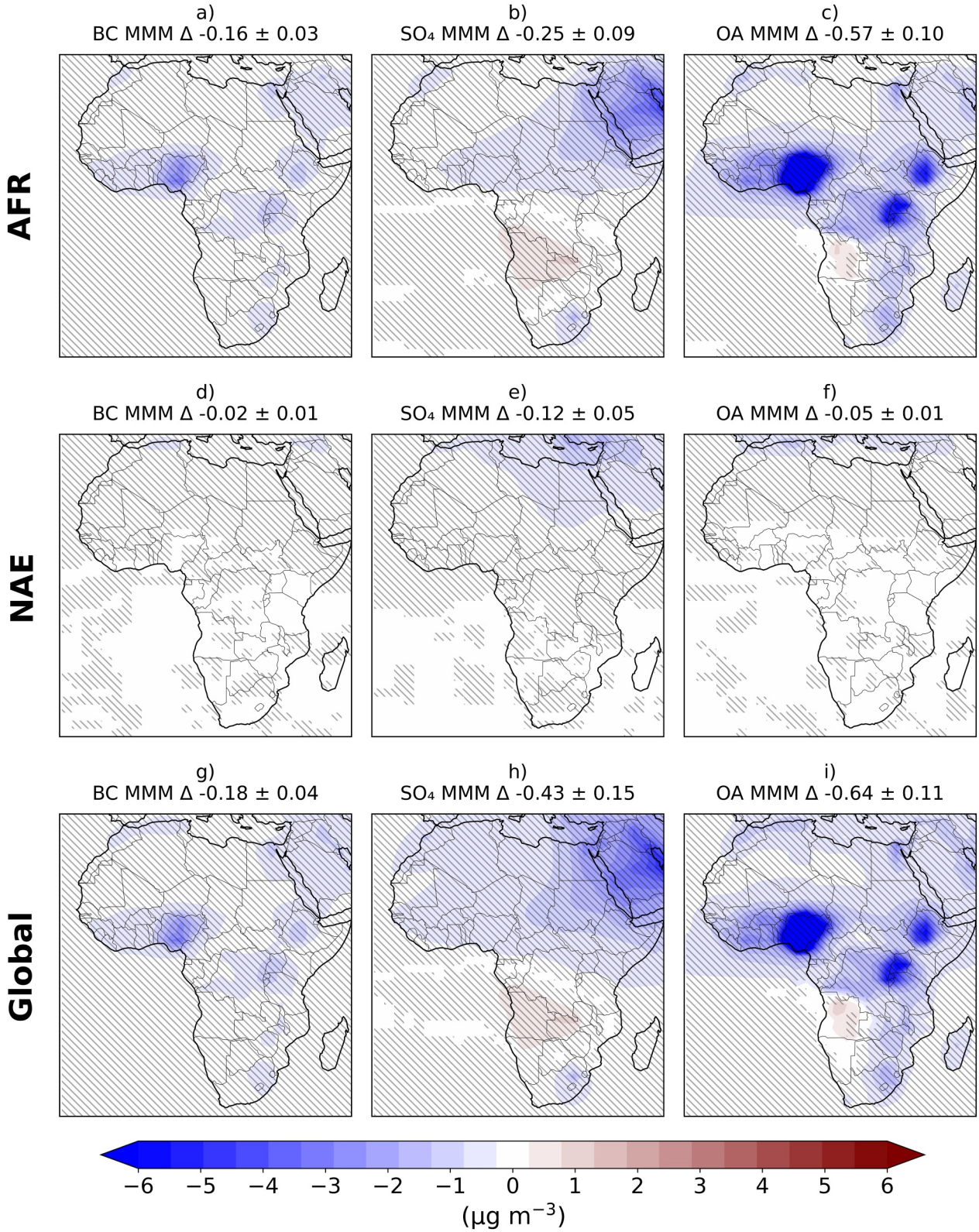

Figure 3. Multi-model mean anthropogenic aerosol changes for the period 2030–2049 for BC (a, d, and g), SO_4 (b, e, and h), and OA (c, f, and i), shown as differences between each regional perturbation simulation and the baseline simulation. Numbers at the top of each subplot indicate the annual average over Africa for the variable in that panel. Hatching indicates regions where ≥70% of models agree on the sign of the change.

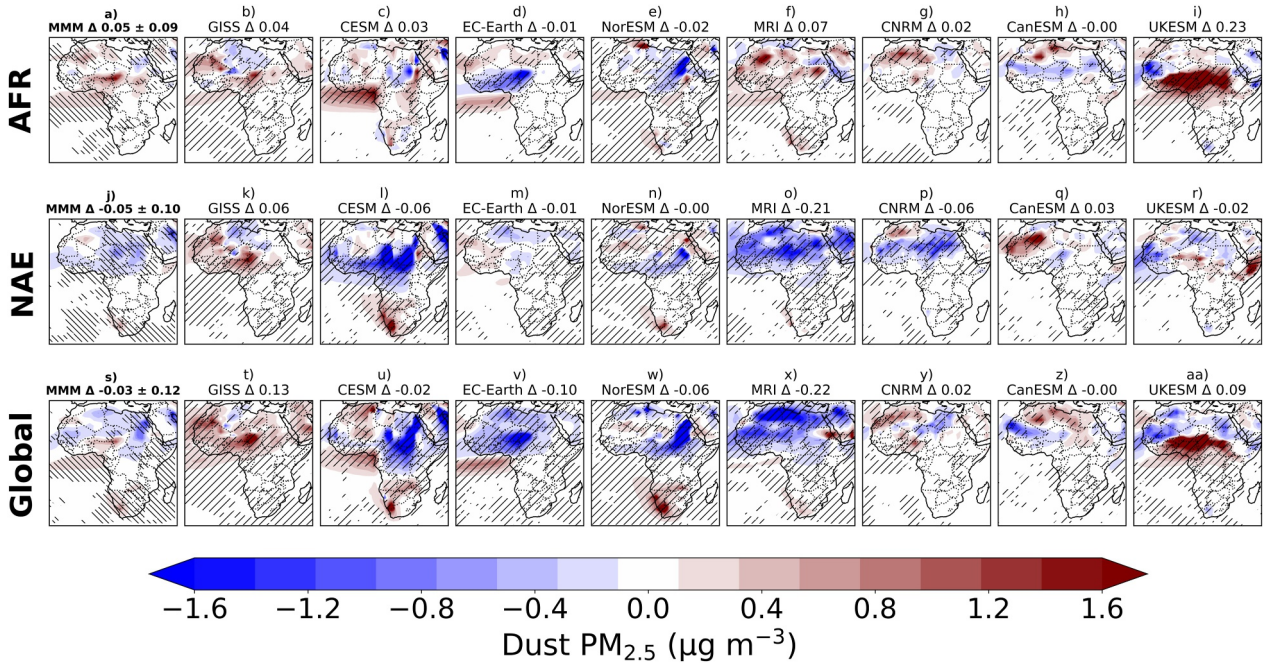

Figure 4. Annual mean dust $PM_{2.5}$ changes for the period 2030–2049, shown as differences between each regional perturbation simulation and the baseline simulation. Numbers at the top of each subplot indicate average annual dust $PM_{2.5}$ changes over Africa. Hatching in MMM (left column) indicates regions where ≥70% of models agree on the sign of the change. Hatching in the individual model panels indicates regions where ≥70% of ensemble members agree on the sign of the change.

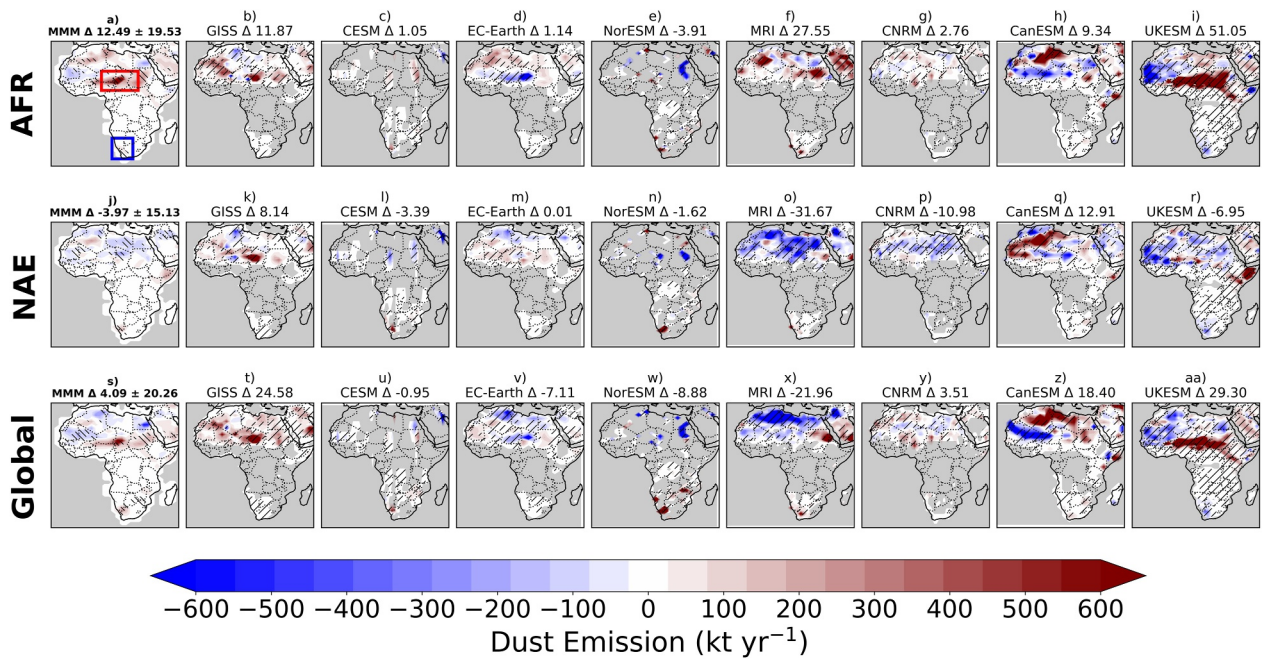

Figure 5. Annual mean dust emissions changes for the period 2030–2049, shown as differences between each regional perturbation simulation and the baseline simulation. Panels (a, j, and s) show MMM $PM_{2.5}$ responses, while panels (b–i, k–r, t–z, and aa) show individual model $PM_{2.5}$ responses. Numbers at the top of each subplot indicate average annual dust emission changes over Africa. Hatching in MMM (left column) indicates regions where ≥70% of models agree on the sign of the change. Hatching in the individual model panels indicates regions where ≥70% of ensemble members agree on the sign of the change. Red and black rectangles in panel a) indicate the definitions of the Chad/Bodélé and Namib desert regions, respectively, as used in this study. Gray areas indicate regions where both baseline dust emissions and dust emission changes are exactly zero.

EC-Earth, 8.88 Kt yr^{-1} in NorESM, and 21.96 Kt yr^{-1} in MRI; Figure 1r) in response to Global anthropogenic aerosol emissions reductions correspond to the largest reductions in dust $PM_{2.5}$ (0.10, 0.06, and 0.22 μg m^{-3}, respectively; Figure 1o), which in turn yield the largest overall $PM_{2.5}$ reductions (1.77, 1.40, and 2.27 μg m^{-3}; Figure 1c). Conversely, the largest absolute increases in dust emissions in response to anthropogenic aerosol forcing (27.55 Kt yr^{-1} in MRI and 51.05 Kt yr^{-1} in UKESM; Figure 1p) under the AFR perturbations correspond to the largest increases in dust $PM_{2.5}$ (0.07 μg m^{-3} and 0.23 μg m^{-3}; Figure 1m), which in turn influence the magnitude of the continental-average $PM_{2.5}$ decreases (0.92 and 0.86 μg m^{-3}; Figure 1a). Notably, the model with the largest absolute change does not necessarily show the largest relative change (Figure S9 in Supporting Information S1). Here, relative change is defined as the change in $PM_{2.5}$ or dust normalized by the baseline value expressed as a percentage, which emphasizes the proportional sensitivity of each model to anthropogenic aerosol reductions. Absolute changes, in contrast, reflect the magnitude of baseline dust emissions and concentrations (Figures S9–S12 in Supporting Information S1). The high coefficients of determination ($R^2 \geq 0.85$ across panels; Figure S9 in Supporting Information S1) indicate that concentration responses scale approximately linearly with emission perturbations, suggesting that inter-model spread is primarily driven by differences in response magnitude rather than nonlinear or meteorological amplification effects.

Although continental-average dust emission changes from regional and global anthropogenic aerosol reductions in individual models range from −1.8% to +2.7% (Figure S9 in Supporting Information S1), key source regions exhibit much larger fractional responses, reaching ±30% in the Sahara and ±25% in the Namib, depending on the model and perturbation. The geographic extent of dust source regions does not change, but the intensity of dust emissions within them varies substantially. As further discussed below in Section 3.2, reductions in anthropogenic aerosols alter climate variables (Hienola et al., 2018; Kloster et al., 2010; Salzmann, 2016; Samset et al., 2018; Westervelt et al., 2018), which in turn enhance dust emissions (Knippertz & Todd, 2012; Miller & Tegen, 1998; Wang & Zhang, 2024) and partially offset possible $PM_{2.5}$ decreases from anthropogenic aerosol emissions reductions.

To better understand the temporal dynamics of this effect, we examine the seasonal cycle of dust emission changes driven by anthropogenic aerosol reductions (Figure S13 in Supporting Information S1). Sahara dust emissions changes show their highest mean values during December–February (DJF) and lower mean values during June–September (JJAS), while the Namib exhibits the opposite pattern, consistent with Zhao et al. (2022). Consequently, African dust emissions are generally lower in JJAS than DJF, though elevated Namib emissions partly counter this seasonal minimum. However, the Sahara contributes most strongly to the overall magnitude of dust emission changes across the continent (Figures S14–S17 in Supporting Information S1). Importantly, this seasonal pattern of aerosol-driven emission changes differs from the typical summer-dominated dust regime in individual future simulations, which generally peak during local summer (JJAS) due to the activation of southern Sahara and Sahel sources (Heinold et al., 2016). The winter maximum in the anthropogenic aerosol-driven dust response is consistent with the baseline seasonal cycle, suggesting that anthropogenic aerosol reductions amplify dust emissions during the climatologically dominant dust season. Haboobs, or density currents spreading outward from convective downdrafts, make a significant contribution to dust emissions in the Sahara during the summer (Allen et al., 2013; Caton Harrison et al., 2019). Global CMIP-class models are incapable of representing this process (Garcia-Carreras et al., 2021), meaning that the sensitivity of dust emissions to anthropogenic aerosols likely misses this intermediary mechanism, which is strongest during the rainy season. Consequently, the seasonal cycle of the modeled anthropogenic aerosol-driven dust response may be distorted, with summer contributions underestimated and winter peaks overemphasized.

3.2. Meteorological Response From Anthropogenic Aerosol Changes and Feedbacks on Dust Emissions

3.2.1. Precipitation and Surface Wind Speed Responses

An overview of the MMM and individual model responses of precipitation and surface wind speed across the AFR, NAE, and Global perturbations is shown in Figure 6, which summarizes the magnitude of ensemble responses and associated uncertainties across models. Over the dust source regions (the Sahara and Namib deserts), precipitation shows a mean positive response of 0.04 ± 0.09 mm day^{-1} (2%) for AFR reductions, 0.03 ± 0.06 mm day^{-1} (2%) for NAE reductions, and 0.05 ± 0.12 mm day^{-1} (3%) for Global reductions (Figures 6a–6c, leftmost bars). However, these responses are not robust given the magnitude of the uncertainties.

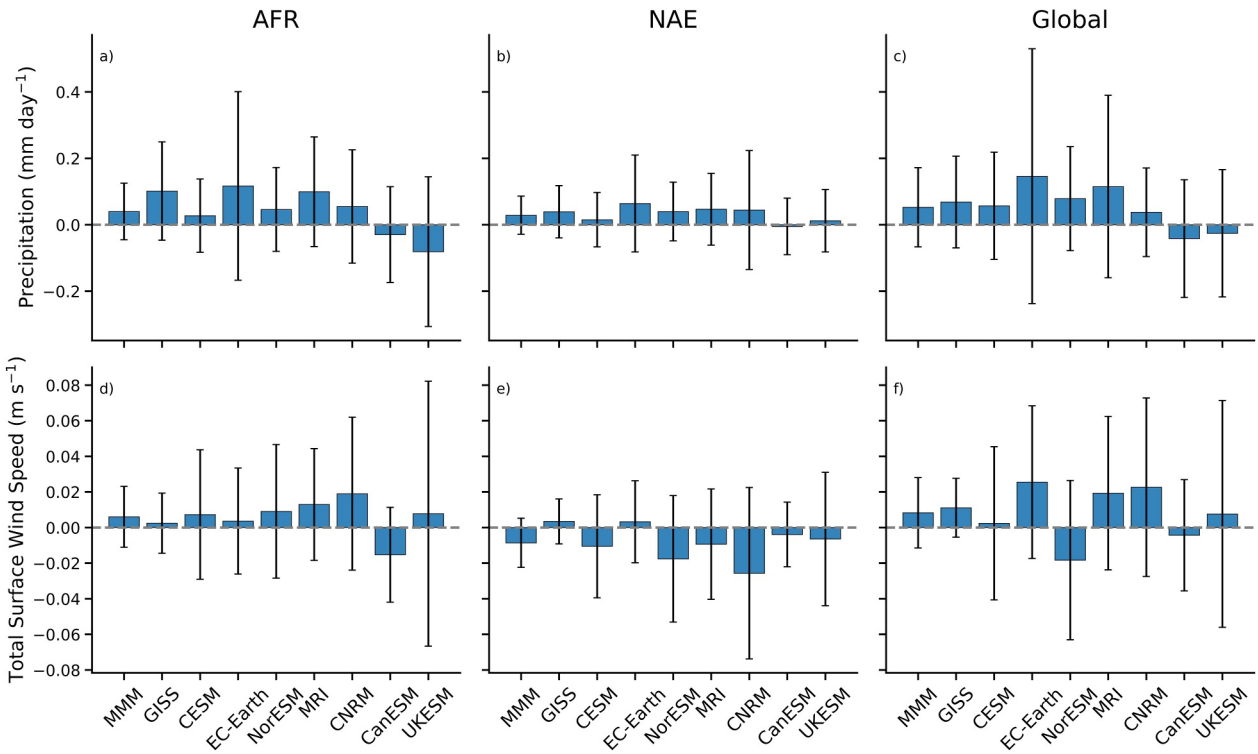

Figure 6. Aggregated summary of MMM and individual model responses to precipitation and wind speed responses across regional perturbation experiments. Precipitation is averaged over the combined Sahara and Namib desert regions (defined in Figure S7 of Supporting Information S1). Surface wind speed is domain-averaged and weighted by dust emission anomalies. Bar charts show the MMM (leftmost bar in each panel) and individual model responses for precipitation and surface wind speed responses across AFR, NAE, and Global perturbations. Error bars denote the inter-model standard deviation for the MMM and the intra-ensemble member uncertainty for individual models.

In contrast, clear and more robust MMM signals are seen in the Sahel (Figure 7, left column). Precipitation increases in the Sahel by 0.27 ± 0.12 mm day^{-1} (6%) under Global aerosol reductions, 0.20 ± 0.11 mm day^{-1} (4%) under AFR reductions, and 0.10 ± 0.07 mm day^{-1} (2%) under NAE reductions. Earlier work has demonstrated that anthropogenic aerosol emission reductions in NAE warm the Northern Hemisphere, shifting the strength and position of the ITCZ and leading to enhanced rainfall over the Sahel (Guo et al., 2024; Hirasawa et al., 2022; Monerie et al., 2023; Toolan, Amooli, et al., 2025; Undorf et al., 2018; Westervelt et al., 2017, 2018). The MMM JJAS precipitation changes help explain part of the MMM dust emission and dust $PM_{2.5}$ patterns shown in Figures 4 and 5. Although precipitation increases over the Sahel, the increase over Chad and Sudan, including the Bodélé Depression, is minimal. This limited wetting in the core dust source region aligns with the MMM increases in dust emissions and dust $PM_{2.5}$ in that area.

With the MMM patterns as context, we examine individual model JJAS precipitation responses. Figure 6 summarizes the inter-model variability in magnitude, while Figure 7 shows the corresponding spatial patterns. Spatially, several models (GISS, CESM, EC-Earth, NorESM, MRI, and CNRM) broadly reproduce the characteristic MMM pattern of enhanced Sahel rainfall and drying south of the equator across all perturbations. These models capture the regional dipole structure and the northward shift of rainfall present in the MMM, though with varying magnitudes. In contrast, CanESM and UKESM consistently depart from the MMM, exhibiting widespread drying over the Sahel where the MMM indicates wetting. Their spatial anomalies are opposite in sign over key regions, and this disagreement persists across AFR, NAE, and Global perturbations.

In addition to departures from the MMM, substantial inter-model variability exists in the magnitude and spatial distribution of Sahel precipitation changes across models. For instance, in the Sahel, GISS, EC-Earth, NorESM, and MRI projects, precipitation increases up to 0.5 mm day^{-1} (5%) under AFR and Global reductions, while the CanESM and UKESM projects decrease up to 0.4 mm day^{-1} (4%), and CESM and CNRM exhibit mixed responses. Under NAE perturbations, most models (GISS, CESM, EC-Earth, NorESM, MRI, and UKESM) show

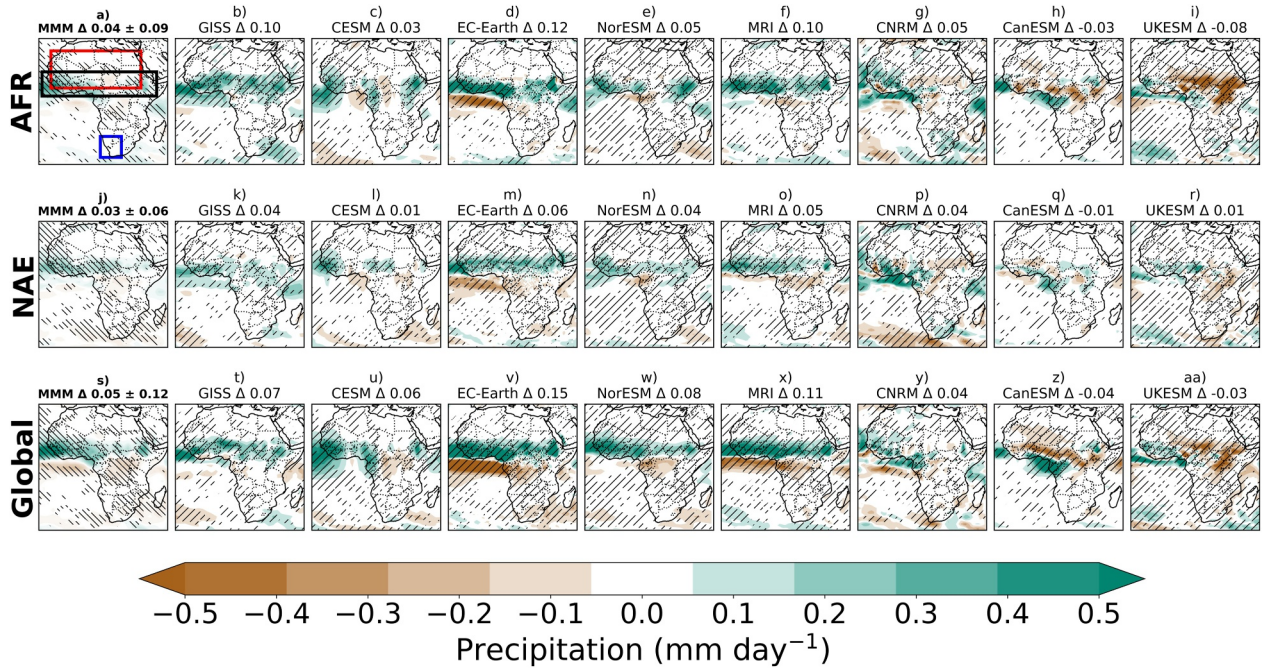

Figure 7. JJAS mean precipitation response to aerosol emission perturbations for 2030–2049, shown as differences between each regional perturbation simulation and the baseline simulation. Panels (a, j, and s) show MMM precipitation responses, while panels (b–i, k–r, t–z, and aa) show individual model precipitation responses. Numbers at the top of each subplot indicate average JJAS precipitation response over the Sahara and Namib deserts combined. Hatching in MMM (left column) indicates regions where ≥70% of models agree on the sign of the change. Hatching in the individual model panels indicates regions where ≥70% of ensemble members agree on the sign of the change. Red, blue, and black rectangles in panel a) indicate the Sahara, Namib, and Sahel regions, respectively, used for regional averaging.

precipitation increases in the Sahel, whereas CNRM and CanESM show both increases and decreases across different parts of the Sahel. The spatial pattern of JJAS precipitation is broadly similar to the annual mean (Figure S18 in Supporting Information S1), suggesting that March-May (MAM) and October-December (OND) precipitation in East Africa does not substantially alter the overall pattern. Strong JJAS precipitation increases under Global aerosol reductions in the Sahel in EC-Earth, NorESM, and MRI correspond to strong decreases in dust emissions, dust $PM_{2.5}$, and overall $PM_{2.5}$ in the Sahara. Conversely, JJAS precipitation decreases in the Sahel in CanESM and UKESM under Global anthropogenic aerosol reductions correspond to strong increases in dust emissions and $PM_{2.5}$. This relationship is not strictly one-to-one due to long-range transport spreading dust across wider regions. Nevertheless, the Pearson correlations in Figure S19 of Supporting Information S1 between model precipitation and dust emissions during JJAS show that wetter monsoons suppress dust in key source regions, with r values up to −0.7 (R^2 = 0.49). Higher soil moisture and partial vegetation growth from the West African monsoon reduce the availability of erodible materials, lowering dust emissions. However, in the Namib Desert, changes in dust emissions are highest in summer (Figures S13, S14, and S16 in Supporting Information S1). Observationally, Prospero and Lamb (2003) showed that dust arrival at Barbados was anticorrelated with rainfall during the preceding summer, implying vegetation feedback. Aerosol Robotic Network (AERONET) observations indicate that this anticorrelation has weakened over the past two decades, as dust exports from Africa to the Atlantic now peak in early summer, largely due to strong transport by the African Easterly Jet (AEJ) and the long atmospheric lifetime of dust, rather than local precipitation patterns (Ridley et al., 2012; Wang et al., 2023).

In our model results, the typical negative rainfall–dust feedback is still evident in most regions of the Sahel, where wetter JJAS monsoons suppress dust emissions. However, EC-Earth and CanESM show positive correlations in some areas, especially in very dry regions, such as Northern Africa, where rainfall is minimal, with r values up to 0.6 (R^2 = 0.36; Figures S19c and S19g in Supporting Information S1). These local deviations do not contradict the broader pattern but highlight the complexity and model dependency of aerosol-precipitation-dust interactions. Beyond transport by the AEJ, dust itself can influence precipitation through its lower single scattering albedo over bright surfaces such as the Sahara (Mahowald et al., 2010; Miller et al., 2014). By reflecting incoming solar radiation, dust reduces the net energy available in convective regions such as the Sahel during the summer. This

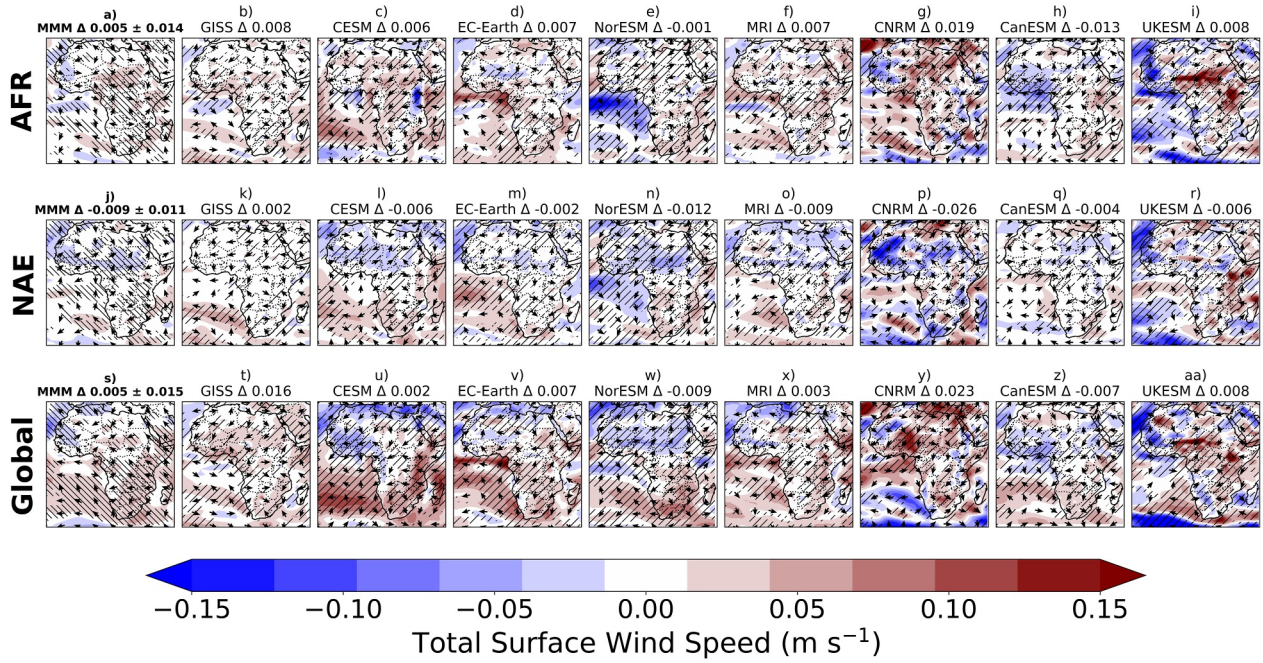

Figure 8. Annual mean total surface wind speed response to aerosol emission perturbations for 2030–2049, shown as differences between each regional perturbation simulation and the baseline simulation. Panels (a, j, and s) show MMM surface wind speed responses, while panels (b–i, k–r, t–z, and aa) show individual model surface wind speed responses. Numbers at the top of each subplot indicate emission-weighted average annual surface wind speed response over Africa. Hatching in MMM (left column) indicates regions where ≥70% of models agree on the sign of the change. Hatching in the individual model panels indicates regions where ≥70% of ensemble members agree on the sign of the change. The wind vectors indicate direction only; magnitudes are represented by the shading.

decrease in energy weakens the local circulation associated with the ITCZ, reducing low-level moisture transport and precipitation (Miller et al., 2014). This creates a feedback loop that can either amplify or dampen local dust concentrations.

We next present the multi-model mean response of annual surface wind speed to anthropogenic aerosol emission reductions in each perturbation. Figure 6 summarizes the continental-average magnitudes, while Figure 8 (left column) shows the corresponding spatial patterns. Surface wind speed changes are weighted by dust anomalies, giving greater influence to regions with higher dust emissions. Continental-average surface winds show very small responses, with changes of 0.005 ± 0.014 m s^{-1} (0.2%) under AFR reductions and 0.005 ± 0.015 m s^{-1} (0.2%) under Global reductions, whereas NAE reductions lead to a small decrease of 0.009 ± 0.011 m s^{-1} (0.3%) (Figures 6d–6f, leftmost bars). These changes are small relative to the ensemble uncertainty and are not robust across models. Wind directions reflect the northward shift of the ITCZ, with southwesterlies and northeasterlies converging further north under NAE and global perturbations. The MMM surface wind speed changes help explain several features of the MMM dust emission and dust $PM_{2.5}$ patterns shown in Figures 4 and 5. In particular, the increase in surface wind speed over Chad and Sudan, including the Bodélé Depression, under the AFR and Global perturbations aligns with the MMM increases in dust emissions and dust $PM_{2.5}$ in this region.

With the MMM patterns established, we examine individual model annual surface wind speed responses (Figures 6 and 8). Spatially, several models (GISS, CESM, EC-Earth, MRI, CNRM, CanESM, and UKESM) reproduce the key MMM circulation features across forcing regions, including strengthened easterlies over northern Africa and alternating bands of wind-speed increases and decreases across the equatorial Atlantic Ocean, though often with stronger intensities compared to the MMM. In contrast, NorESM consistently departs from the MMM, generating much stronger and more spatially extensive wind anomalies under all perturbations.

Aside from deviations from the MMM, substantial inter-model variability exists in the magnitude and spatial distribution of surface wind speed changes across models. Most models project increases of up to 0.15 m s^{-1} (4%) over the Sahara (dominated by northeasterly winds), parts of West Africa (southwesterlies), and southern/eastern Africa (southeasterlies), though the magnitude and spatial pattern vary considerably by model and perturbation region. For instance, under AFR reductions, slightly more than half of the models project overall continental

increases except NorESM, CanESM, and UKESM, while under Global reductions, increases are simulated in all models except NorESM and UKESM. This inter-model variability means that some models simulate surface wind speed increases in the Sahel while others project decreases. Most models show that increases in surface wind speed are spatially associated with enhanced dust emissions, dust $PM_{2.5}$, and total $PM_{2.5}$, particularly over the Sahara and Namib deserts. For example, NorESM projects surface wind speed increases of up to 0.10 m s^{-1} (3%) under the Global perturbations across the Namib Desert (Figure 8w), corresponding to increases in dust emissions and $PM_{2.5}$, with similar relationships seen in CESM and UKESM (over the Bodélé Depression). The correlation is further quantified in Figure S20 of Supporting Information S1: surface wind speed correlates strongly with dust emissions, reaching $r = 0.9$ ($R^2 = 0.81$) across much of the Sahara and Namib deserts in most models.

The physical mechanisms underlying these relationships are well established. Aerosols cool the surface by reflecting sunlight and increasing cloudiness via CCN effects, which lower wind speeds by making the boundary layer more stable and reducing both turbulence and momentum mixing (Engelstaedter et al., 2006; Jacobson & Kaufman, 2006; Miller, Perlwitz, & Tegen, 2004; Pu & Ginoux, 2017; Zender & Kwon, 2005). Removing aerosols allows more solar radiation to reach the surface, warming the land, strengthening pressure gradients, and enhancing boundary-layer mixing. This, in turn, accelerates near-surface winds and enhances dust generation, creating a local dust–radiation–planetary boundary-layer mixing–emission feedback (Ahn et al., 2007; Heinold et al., 2007). Regional changes in surface pressure gradients also occur, but these are more complex, less predictable, and likely more model-dependent. Indeed, Evan (2018) showed that over barren regions such as the Sahara, inter-model differences in dust emissions are primarily driven by differences in how models represent surface wind speed.

3.2.2. Regression Analysis of Dust Emissions and Meteorological Drivers in GISS-E2-1-G

To disentangle the sensitivity of dust emissions to and the relative importance of meteorological drivers, we applied a multiple linear regression of annual dust emission changes against changes in precipitation, 10 m surface wind speed, threshold velocity for dust emission, and the dry convective velocity scale (Figures 9 and 10; see Section 2.3 for methodological details). The threshold velocity for dust emission is used to assess the influence of soil moisture through its effect on particle cohesion, with wetter soils requiring stronger near-surface wind forcing to initiate dust emission, while the dry convective velocity scale characterizes gustiness and turbulent mixing within the planetary boundary layer. The detailed physical interpretation of these two dust emission metrics and their responses to anthropogenic aerosol reductions are provided in (Figures S21 and S22 of Supporting Information S1). All regression coefficients (β_P for precipitation, β_W for 10 m surface wind speed, β_T for threshold velocity for dust emission, and β_C for dry convective velocity scale) were standardized, so that both the predictors and dust emissions were scaled to zero mean and unit variance prior to regression. This standardization ensures that the coefficients represent the change in dust emissions (in standard deviation units) per one standard deviation change in the predictor, enabling direct comparison across variables with different units and magnitudes of variability. Unlike the pairwise correlations discussed earlier, which reflect the total association of each driver with dust, the regression model isolates the independent contribution of each variable while controlling for the others. Dust emissions are most sensitive in the Sahara and Namib deserts, while sensitivities across the rest of Africa are near zero.

Across Africa, precipitation generally exhibits negative standardized sensitivities in major source regions (Figures 9a, 9e, and 9i), consistent with the established role of rainfall in suppressing dust emissions through enhanced soil moisture and vegetation growth (Cowie et al., 2013; Prospero & Lamb, 2003; Zender & Kwon, 2005). However, the relationship is not spatially uniform: in hyper-arid parts of the Sahara, positive sensitivities of comparable magnitude also emerge. This contrast likely reflects the weak or even reversed dust-precipitation relationship in hyper-arid regions, where rainfall is rare and other processes such as wind speed dominate (Aryal & Evans, 2023; Pu & Ginoux, 2017; Zhao et al., 2022). Not all CMIP6 models include vegetation feedback to climate, which may influence the magnitude and spatial pattern of precipitation-related sensitivities.

Surface wind speed shows positive standardized sensitivities over key dust source regions, but the magnitudes are generally smaller than those of gustiness (Figures 9b, 9f, and 9j). Its spatial pattern is also more localized, with strong positive signals concentrated in well-known emission hotspots such as the Bodélé Depression, northern Mali, and Libya. Threshold velocity for dust emission shows the strongest negative standardized sensitivities

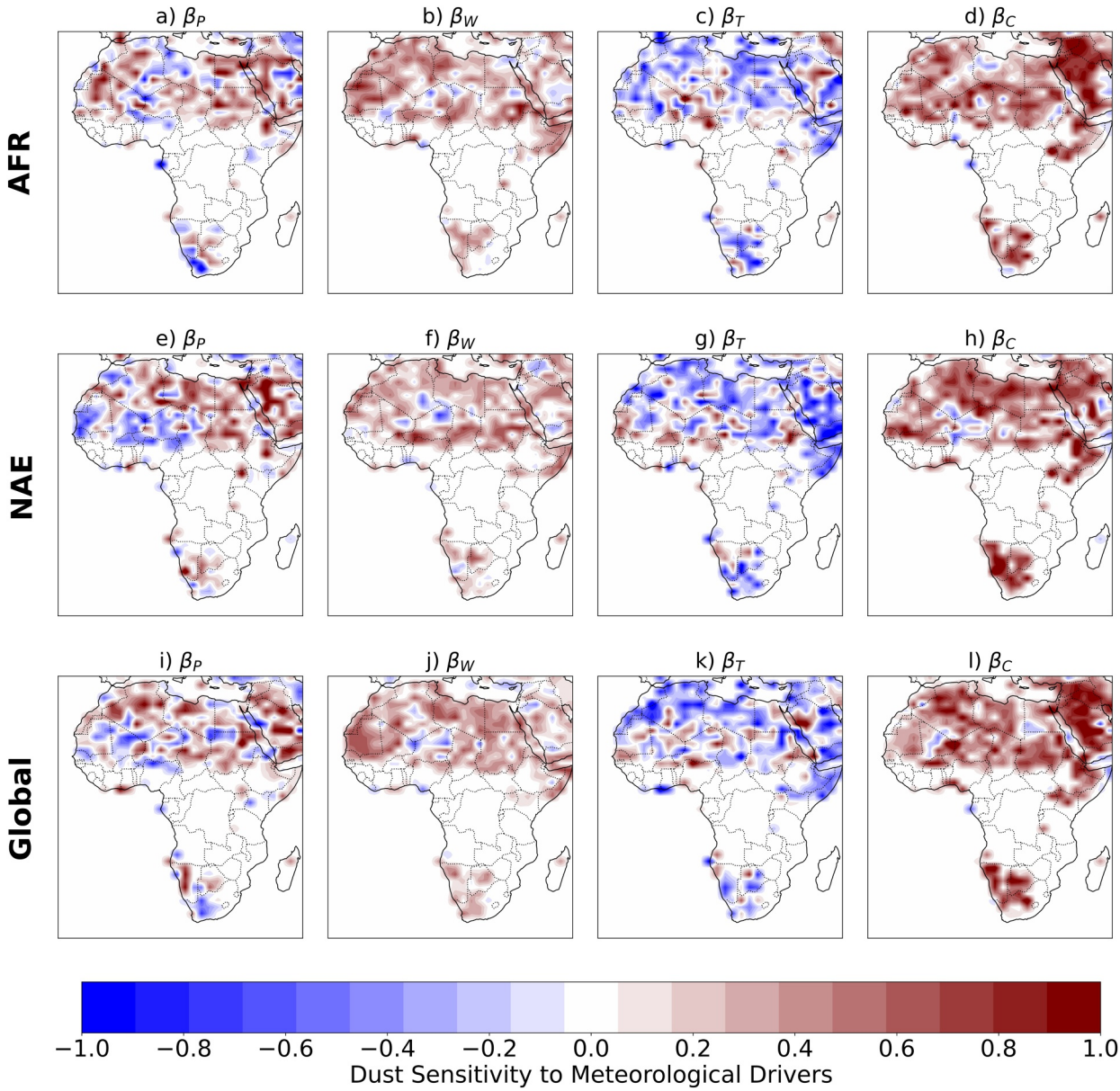

Figure 9. GISS model annual dust emissions sensitivity for the period 2030–2049, shown with respect to annual precipitation (a, e, and i), annual cubed surface total wind speed (b, f, and j), annual threshold velocity for dust emissions (c, g, and k), and annual dry convective velocity scale (d, h, and l). Sensitivities are shown as standardized regression coefficients.

(Figures 9c, 9g, and 9k), consistent with the physical expectation that wetter soils raise the threshold and suppress emissions, while drier soils lower it and enhance dust uplift. The dry convective velocity scale displays strongest positive standardized sensitivities and is spatially uniform across much of the Sahara (Figures 9d, 9h, and 9l), highlighting the importance of turbulent mixing and gustiness in facilitating dust emissions. The model skill is high: the predictors together explain up to 90% ($R^2 = 0.9$) of dust variability across regions, with nRMSE and CvMAE generally below 50% (Figures S23a–S23c in Supporting Information S1). Only isolated regions show errors above this threshold, primarily over major dust source regions where emissions are particularly sensitive to meteorological variability, leading to elevated residuals.

Figure 10 presents the absolute standardized regression coefficients (0–1), highlighting the relative importance of each meteorological driver irrespective of sign. Across all perturbation regions, the dry convective velocity scale emerges as the dominant predictor, followed by threshold velocity, then precipitation, with large-scale surface

wind speed contributing least, though with strong localized contribution in Bodélé Depression, northern Mali, and Libya. Threshold. Regional averages reinforce this hierarchy: the dry convective velocity scale explains the largest fraction of variability (mean absolute standardized coefficient 0.17–0.19), followed by threshold velocity (0.10–0.13), precipitation (<0.13), and wind speed (<0.11) (Figure 10m). Although previous studies for example, Zhao et al. (2022) identify surface wind speed as a dominant driver of dust emissions, our analysis shows that much of its apparent influence is shared with other predictors, particularly the dry convective velocity scale. These two variables covary by as much as 0.6 depending on the perturbation (Figure S24 in Supporting Information S1). Once this shared variance is accounted for in the standardized framework, the independent contribution of mean surface wind speed is reduced, explaining its lower relative importance in the regression ranking. Notably, across all perturbation regions, surface wind speed consistently ranks as the smallest independent contributor among the meteorological drivers, highlighting the dominant role of convective and threshold-related processes.

Most models do not provide in public data repositories the full set of dust emission predictors needed for a complete regression analysis, which limits inter-model comparison. To evaluate how much variance could be explained using only commonly available predictors, we performed a reduced-predictor sensitivity test within GISS and the other models using surface wind speed and precipitation alone (Figure S25 in Supporting Information S1). As expected, the explained variance decreases substantially relative to the full set in GISS; the model struggles to explain 50% of dust emission variability. Only a few models (EC-Earth, MRI, and CNRM) explain up to 70% ($R^2 = 0.7$) of dust emission variability with surface wind speed and precipitation alone but with larger errors and the rest struggle to capture even 50%. This confirms that key processes represented in GISS, particularly wind gustiness and threshold velocity, capture important variability in dust emissions that cannot be reproduced from surface wind speed and precipitation alone.

The full GISS regression results help explain why regions with MMM increases in surface wind speed and gustiness, and decreases in threshold velocity and precipitation, correspond to MMM increases in dust emissions and concentrations, for example, in the Bodélé Depression, and likewise for decreases. However, we do not assume that the quantitative standardized regression coefficients from GISS apply directly to other models. Notably, GISS shows a comparatively similar response between the Global and AFR experiments, with the strongest response under the Global perturbation, distinguishing it from several other models in the ensemble. Differences in dust-emission parameterizations and in the treatment of meteorology can alter both the sign and magnitude of predictor sensitivities. In particular, our finding (Figure 10) that much of the dust emission response to anthropogenic aerosol reductions arises from changes in gustiness highlights a potential blind spot in consensus dust emissions modeling, since few CMIP-class models explicitly represent this mechanism. Also, given the strong role of soil moisture (through its effect on threshold velocity) in driving dust anomalies under anthropogenic aerosol reductions (Figure 10), it is important to highlight a common limitation in how soil moisture is represented in models. While the impact of soil moisture is more broadly included across models, many formulations follow Fécan et al. (1999) and use moisture from the top 5–10 cm of the soil layer. Recent work (e.g., Okin, 2022) suggests that the damping of dust emission actually operates over much shallower depths, on the order of millimeters, with moisture relaxing on hourly timescales after rainfall. This implies that many models have excessive moisture inertia, which delays the resumption of dust emission for too long after precipitation events.

Taken together, these findings suggest that more models should add a representation of wind gustiness and their sensitivity to climate change. While the standardized regression analysis provides useful insight into the relative influence of meteorological drivers on dust emissions, several limitations should be noted. First, standardized coefficients capture relative statistical contributions under the linear model framework and do not fully represent nonlinear or indirect effects (e.g., precipitation influencing threshold velocity). Second, the analysis does not explicitly account for land surface characteristics such as vegetation cover, soil type, and bare ground fraction, which are known to also strongly modulate dust availability and emission potential (Kim et al., 2017; Munson et al., 2011; Pu & Ginoux, 2017). Models do not simulate significant trends in surface bareness over time (Zhao et al., 2022), indicating that bare-soil fraction is largely static in these simulations. Other land-surface characteristics (e.g., vegetation cover, soil type) may exhibit limited or poorly constrained changes (Kok et al., 2023), potentially influencing dust availability in ways not captured by our regression. Land use in all simulations follows the SSP3-7.0 scenario, so changes in vegetation or surface characteristics are consistent across

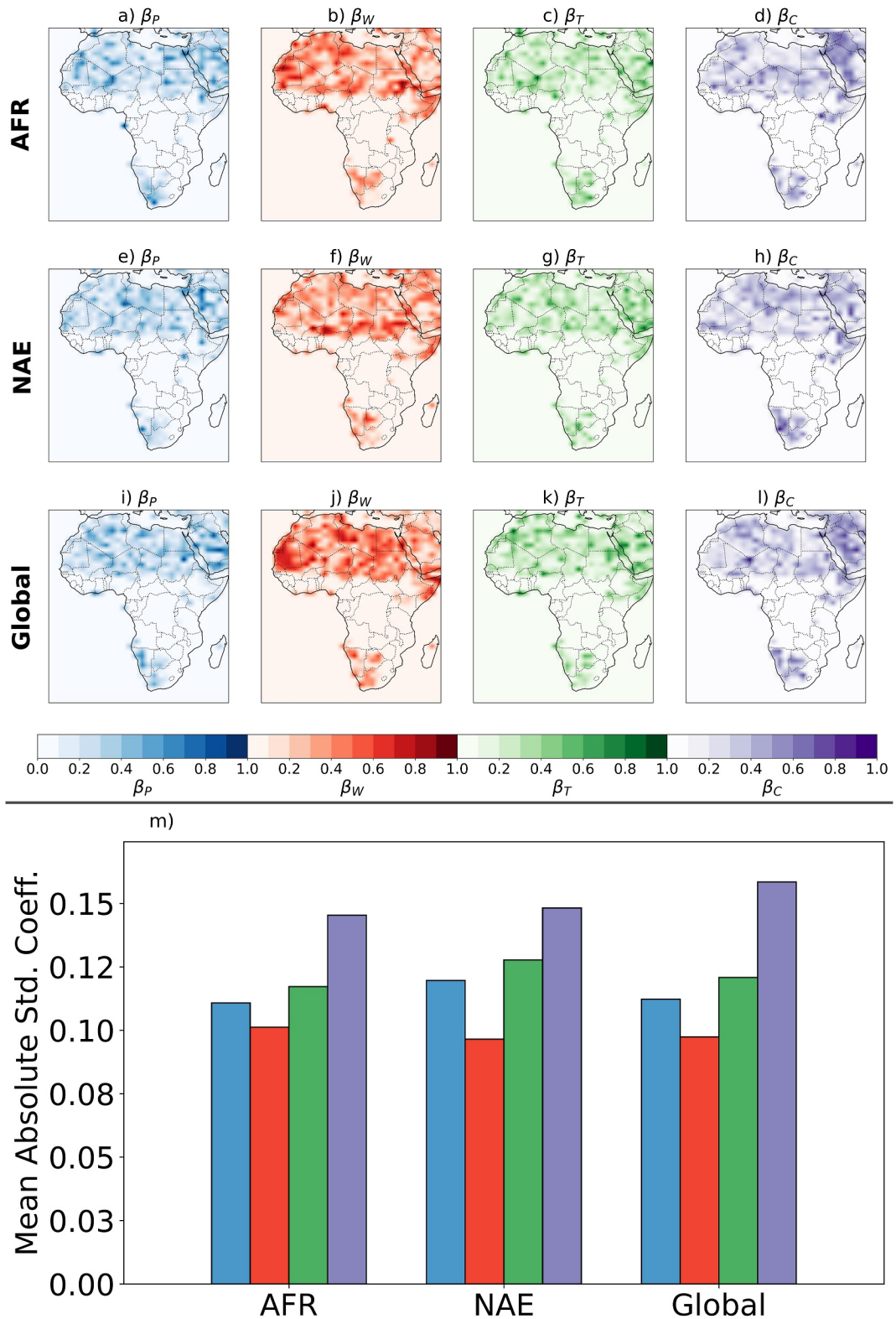

Figure 10. Relative importance of key meteorological drivers of dust emissions from the regression model. Bar charts indicate the average absolute standardized regression coefficient for each regional perturbation.

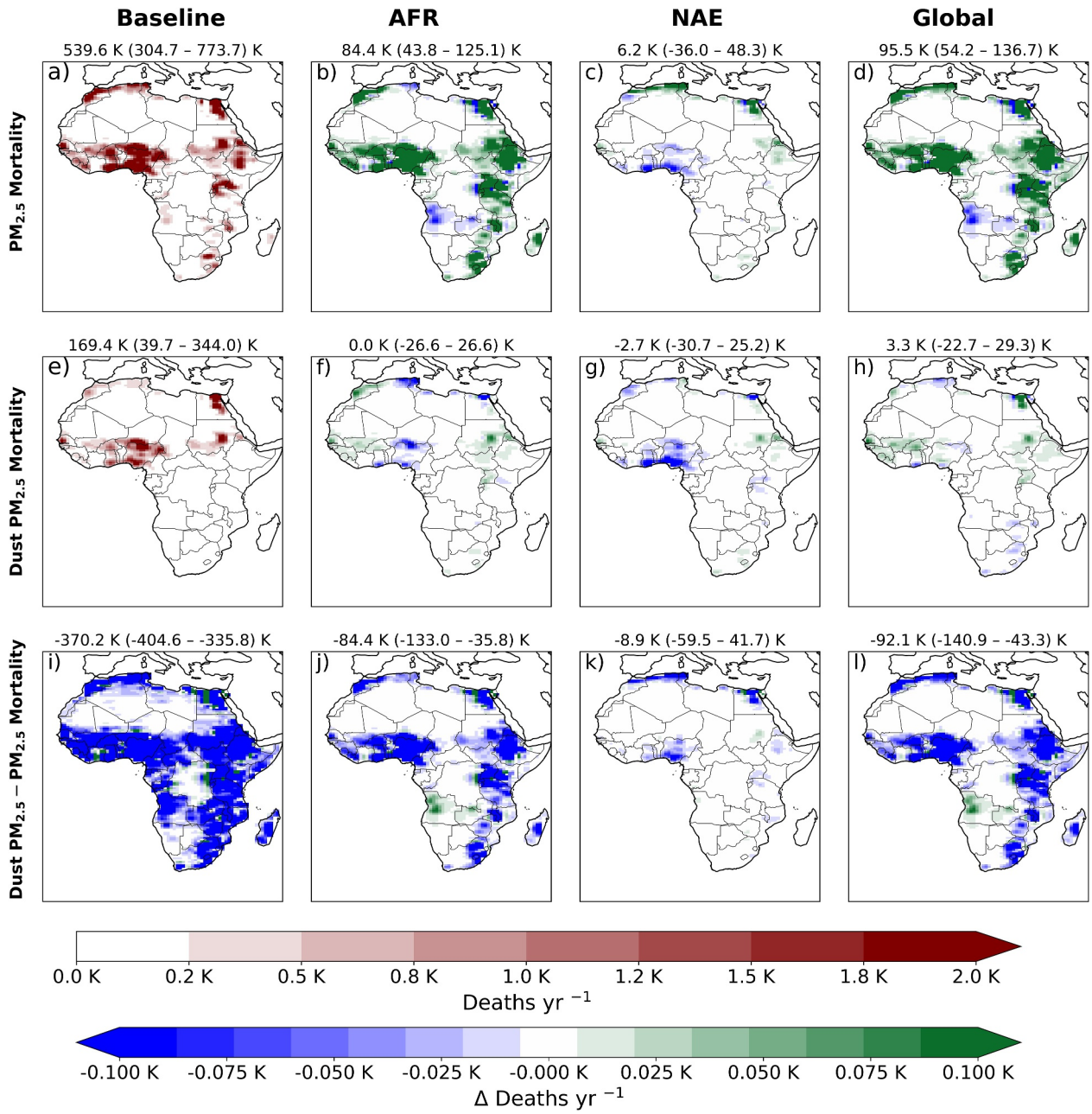

Figure 11. Multi-model mean $PM_{2.5}$- and dust $PM_{2.5}$-attributable deaths across Africa under the baseline simulation (first column) and in response to regional anthropogenic aerosol reduction experiments (remaining columns). Rows show (top) total $PM_{2.5}$-attributable deaths, (middle) dust $PM_{2.5}$-attributable deaths, and (bottom) the difference (dust $PM_{2.5}$ − total $PM_{2.5}$). The values shown in the panel titles represent the total continental deaths summed across Africa, with 95% confidence intervals derived from propagation of inter-model ensemble uncertainty and RR uncertainty. Positive values in the first two rows indicate avoided deaths (relative to the baseline), while negative values indicate additional deaths. In the difference panel (last row), negative values indicate that $PM_{2.5}$-related mortality exceeds dust-related mortality, whereas positive values indicate the opposite.

perturbation experiments (Wilcox et al., 2023); thus, the differences we report are primarily driven by aerosol and meteorology rather than evolving land use.

3.3. Excess Mortality Attributable to Total $PM_{2.5}$ and Dust $PM_{2.5}$

We estimate excess deaths per year attributable to total $PM_{2.5}$ and dust $PM_{2.5}$ (Figure 11) in the baseline and under regional anthropogenic aerosol reduction scenarios for 2050. The difference between the 2030–2049 average

$PM_{2.5}$ concentrations and the 2050 $PM_{2.5}$ concentrations is small; therefore, using 2050 as the representative year does not meaningfully affect the results. Mortality was calculated separately for each model using model-specific $PM_{2.5}$ concentrations and then averaged to obtain the multi-model mean. Because SSP3-7.0 represents a high-population, high-vulnerability future, our absolute mortality estimates should be interpreted as upper-bound values. In a lower-population or healthier socio-economic pathway (SSP1), the same $PM_{2.5}$ changes would produce fewer deaths. Absolute mortality in both the baseline and perturbation scenarios depends on the SSP3-7.0 population, age distribution, and baseline mortality rates, which are held constant between the two scenarios. Therefore, the differences between the baseline and perturbation scenarios (i.e., avoided or additional deaths) reflect only the $PM_{2.5}$ changes driven by anthropogenic aerosol reductions and are independent of demographic assumptions.

At the continental scale, baseline $PM_{2.5}$-related deaths per year are approximately 540,000 (95% CI: 305,000–774,000; Figure 11a), with dust $PM_{2.5}$ alone contributing 169,000 (95% CI: 40,000–344,000), about 31% of the total. The largest $PM_{2.5}$-related and dust $PM_{2.5}$-related deaths are from IHD and stroke, accounting for 28%–37% of mortality depending on the region (Figure S26 in Supporting Information S1). The remaining 63%–72% of $PM_{2.5}$-related and dust $PM_{2.5}$-related deaths are distributed among LC, COPD, T2DM, and ALRI. Similar cause-specific relative contributions are expected because the same RR functions are applied to both dust and total $PM_{2.5}$. The dominance of cardiovascular pathways in $PM_{2.5}$- and dust $PM_{2.5}$-attributable mortality reflects the structure of the underlying GBD exposure–response functions rather than a novel model outcome.

The previous paragraph describes continental absolute $PM_{2.5}$- and dust $PM_{2.5}$-attributable deaths, which depend on SSP3-7.0 demographic assumptions. We now focus on the differences between scenarios, which isolate the health impacts of $PM_{2.5}$ changes from anthropogenic aerosol reductions alone (no population effects). Nonetheless, the largest avoided or additional deaths still occur in highly populated regions where $PM_{2.5}$ and dust $PM_{2.5}$ changes affect more people. Dust $PM_{2.5}$ either offsets or amplifies $PM_{2.5}$-related avoided deaths from anthropogenic aerosol emission reductions, depending on the scenario. Across Africa, dust $PM_{2.5}$ accounts for 3,300 (95% CI: −23%,000%–29%,000%; 3.4%) of 96,000 (95% CI: 54,000–137,000) avoided $PM_{2.5}$-related deaths per year under Global anthropogenic aerosol emissions reductions (Figures 11d and 11h), indicating that most health benefits stem from reductions in anthropogenic sources. Under AFR reductions, 84,000 (95% CI: 43,000–125,000) deaths per year are avoided, while dust related $PM_{2.5}$ changes produce no net mortality effect at the continental scale. Finally, in NAE reductions, 6,000 (95% CI: −36,000–48,000) $PM_{2.5}$-related deaths per year are avoided, with dust offsetting 2,700 (95% CI: −31%, 000%–25%, 000%; 45%), although this effect is not statistically distinguishable from zero. The comparatively small absolute dust contribution likely reflects the limited spatial overlap between peak dust concentrations and densely populated areas, although relative offsets may appear large in scenarios where total $PM_{2.5}$ benefits are modest.

We next examine the regional distribution of baseline $PM_{2.5}$- and dust $PM_{2.5}$-related deaths and scenario-driven changes under anthropogenic aerosol reductions (Figure 12). Regionally, baseline $PM_{2.5}$-related deaths are highest in Western and Northern Africa, followed by Eastern, Central, and Southern Africa (Figure 12a). Dust $PM_{2.5}$-related deaths in the baseline show a similar regional pattern, with Western Africa again having the largest burden (Figure 12c). The high mortality in Western Africa reflects population growth under SSP3-7.0, while Northern Africa's burden is amplified by an older population structure by 2050, with the largest impacts occurring in populous countries such as Nigeria, Egypt, and Sudan (Amooli et al., 2025; Im et al., 2023; Figure S29 in Supporting Information S1). Southern Africa experiences nearly zero dust-related deaths per year, while $PM_{2.5}$ deaths remain nonzero, indicating that mortality is primarily driven by anthropogenic sources. Although baseline dust-related deaths are near zero in this region, small changes in dust concentrations under perturbation scenarios can still amplify or offset $PM_{2.5}$-related avoided deaths due to overlaps with population distribution and nonlinear exposure–response effects.

Regionally, under Global anthropogenic aerosol reductions, $PM_{2.5}$-related avoided deaths are highest in Northern Africa (33,000), followed by Eastern (29,000), Western (28,000), Southern (4,400), and Central Africa (1,100) (Figure 12b). Dust $PM_{2.5}$ amplifies $PM_{2.5}$-related avoided deaths in Eastern, Northern, and Western Africa (3%–6%), but offsets them in Central Africa (4%) and Southern Africa (11%) (Figure 12d). Under AFR reductions, $PM_{2.5}$-related avoided deaths show a broadly similar regional distribution, with Western Africa leading (28,000), followed by Eastern and Northern Africa (Figure 12b). Dust $PM_{2.5}$ amplifies $PM_{2.5}$-related avoided deaths in Eastern and Southern Africa (2%–5%) but offsets them in Western, Northern, and Central Africa

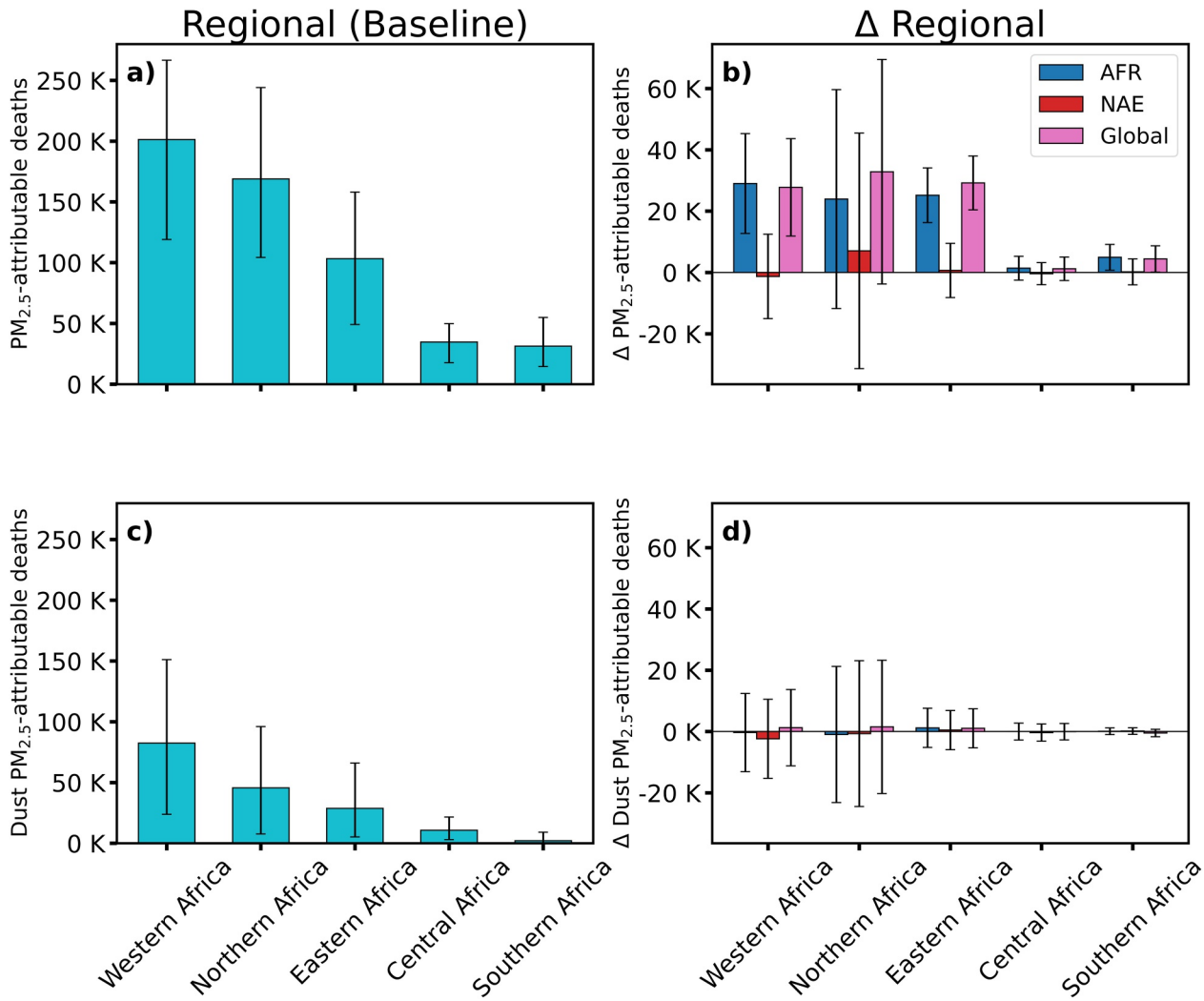

Figure 12. $PM_{2.5}$- and dust $PM_{2.5}$-attributable deaths across African subregions under the baseline simulation and in response to regional anthropogenic aerosol reduction experiments. The first row shows total $PM_{2.5}$-attributable deaths, and the second row shows dust $PM_{2.5}$-attributable deaths. Panels (a, c) present mortality estimates for $PM_{2.5}$ and dust $PM_{2.5}$, respectively, under the baseline simulation. Panels (b and d) show the corresponding changes in deaths under the regional anthropogenic aerosol reduction experiments. Bars represent subregional total deaths, and error bars indicate 95% confidence intervals derived from the propagation of inter-model ensemble uncertainty and RR uncertainty. Regional definitions are shown in Figure S30 of Supporting Information S1.

(1%–4%) (Figure 12d). Under NAE reductions, $PM_{2.5}$-related avoided deaths occur only in Northern Africa (7,000), likely due to reduced transport of high aerosol concentrations from Europe, while other regions experience $PM_{2.5}$-related additional deaths (Figure 12b). Dust $PM_{2.5}$ strongly contributes to these additional deaths (83%–182%) and offsets 10% of $PM_{2.5}$-related avoided deaths in Northern Africa. However, dust $PM_{2.5}$-attributable mortality estimates are generally small relative to their uncertainties and should be interpreted with caution. Overall, these patterns of mortality changes align with multi-model mean $PM_{2.5}$ and dust $PM_{2.5}$ concentrations (Figures 2 and 4). In the dust $PM_{2.5}$ − total $PM_{2.5}$ difference panel (Figure 11, last row), positive values observed in parts of southern and central Africa (e.g., Angola, Zambia, and the Democratic Republic of the Congo) indicate regions where dust-attributable mortality exceeds the non-dust component of $PM_{2.5}$, suggesting a dominant relative role of dust in these areas under the AFR and Global reduction scenarios. Overall, despite these localized regions, non-dust $PM_{2.5}$ remains the primary driver of PM-related mortality across most of the African continent in both the baseline and reduction scenarios.

Our baseline estimate of 540,000 $PM_{2.5}$-attributable deaths per year in Africa, calculated using SSP3 2050 population, age distribution, and baseline mortality, is consistent with mid-century projections (0.5–1 million deaths) (Amooli et al., 2025; Chowdhury et al., 2020, 2023; Shindell et al., 2022). It is also higher than current

ambient $PM_{2.5}$ mortality (383,000 deaths per year; Murray et al., 2020), reflecting demographic changes under the SSP3 pathway. The difference in magnitude relative to some previous studies is partly because we use a multi-model mean across ensemble simulations, whereas several earlier studies report individual model estimates. The total uncertainty, which combines inter-model spread and uncertainty in the RR function, has an upper bound of nearly 774,000 deaths per year, encapsulating many estimates in single model studies. Bauer et al. (2019) estimated that air pollution in Africa causes approximately 800,000 premature deaths annually, with $PM_{2.5}$ responsible for two-thirds of these and gaseous pollutants, mainly ozone, for the rest. Lelieveld et al. (2015) reported 273,000 premature deaths in 2010 from $PM_{2.5}$ and ozone, noting desert dust as a major contributor. Similarly, Amooli et al. (2025), Shindell et al. (2022), Wells et al. (2024) projected that thousands of $PM_{2.5}$-attributable deaths in Africa could be avoided under low-emission scenarios.

In our study, dust contributes roughly 31% to baseline $PM_{2.5}$ mortality, consistent with previous assessments: Aboagye-Okyere et al. (2025) estimated dust currently contributes 36% of $PM_{2.5}$-attributable deaths in Africa; globally, Evans et al. (2013) estimated 33%, Yang et al. (2022) 22%, and Lelieveld et al. (2015) 18%, with differences largely driven by assumptions about dust toxicity. Although these studies differ in assumptions and spatial domains, they help contextualize the scale of Africa's $PM_{2.5}$ burden.

The estimated $PM_{2.5}$ and dust $PM_{2.5}$ mortality in this study are subject to notable uncertainties, as reflected by the wide 95% confidence intervals. These uncertainties arise from both the inter-model ensemble spread and the relative risks derived using the MR-BRT function (Figure S27 in Supporting Information S1). For total $PM_{2.5}$-attributable mortality, inter-model variability accounts for approximately 40%–60% of the total uncertainty in both the baseline and anthropogenic aerosol reduction scenarios, with the remaining 40%–60% attributable to uncertainty in the RR functions. In contrast, for dust $PM_{2.5}$-attributable mortality, inter-model spread dominates, contributing roughly 70%–80% of the total uncertainty, while RR uncertainty accounts for 20%–30%. Model agreement on central estimates is limited, particularly in the baseline simulation (Figure S28 in Supporting Information S1). Uncertainty in dust $PM_{2.5}$-related mortality changes is especially high over Northern and Western Africa. This likely reflects limited epidemiological constraints on exposure–response relationships at the high concentrations characteristic of dust-dominated environments as well as substantial inter-model spread in simulating dust levels in these regions. Despite considerable uncertainty in the magnitude of dust offsets, the MMM central estimates of net health benefits remain positive across scenarios, although uncertainty ranges for NAE reductions include zero. Regional differences in model skill in simulating present-day $PM_{2.5}$ variability further influence confidence in projected mortality changes, with higher confidence in Western Africa where models better reproduce observed $PM_{2.5}$ levels and comparatively lower confidence in Eastern Africa, where model performance is weaker (Toolan, Amooli, et al., 2025).

Given that inter-model variability in dust $PM_{2.5}$ responses across Earth System Models dominates the total uncertainty, future work should prioritize improving the representation of aerosol processes in climate models. In addition, reducing uncertainty in the RR function will require substantial cross-disciplinary efforts, including improved estimates of $PM_{2.5}$ exposure and the development of more rigorous concentration-response functions that account for regional and source-specific dependencies through epidemiological cohort studies. Internal variability within individual models may also contribute to uncertainty, although its magnitude is not explicitly quantified here. Our mortality estimates assume equal toxicity across all $PM_{2.5}$ components. However, some studies have explored the possibility that mineral dust may be less harmful per unit mass than anthropogenic aerosols such as BC, SO_4, and OA (Chowdhury et al., 2022; Lelieveld et al., 2015), although the epidemiological evidence remains inconclusive and insufficient to robustly differentiate toxicity by source, consistent with the GBD framework. If future evidence confirms lower toxicity for mineral dust, this simplification could lead to an overestimation of the health burden in cases where dust $PM_{2.5}$ increases while more toxic anthropogenic species decline. Thus, our results may represent a conservative estimate of potential health impacts under the assumption of equal toxicity across $PM_{2.5}$ components.

Nevertheless, our findings highlight the health implications of dust aerosols through meteorological feedbacks from regional anthropogenic aerosol emission reductions. Even under current conditions, natural dust can contribute substantially to $PM_{2.5}$ exposures in Africa and occasionally push concentrations above air quality guideline levels, highlighting its ongoing public health relevance (Bauer et al., 2019; Garrison et al., 2014; Querol et al., 2019). While regional emission reductions generally yield health benefits, feedbacks on dust may modify these gains in some regions, although the magnitude of the effect varies and is subject to uncertainty. This

highlights the importance of mitigation strategies that consider both anthropogenic sources and natural-source feedbacks. For example, greenhouse-gas mitigation can reduce dust emissions by weakening surface winds and stabilizing soils (Clifford, 2019; Gomez et al., 2023), while land-management practices such as vegetation restoration or soil stabilization can directly suppress dust sources (Cowie et al., 2013; Vautard et al., 2010). These considerations help contextualize our findings by showing how policies aimed at both anthropogenic and natural sources can enhance air-quality and health benefits.

4. Conclusion

We used eight Earth System Models (10 ensemble members each) from the RAMIP simulations to assess how African climate and air quality respond to regional and global anthropogenic aerosol emission reductions, with a focus on meteorological feedbacks affecting dust emissions and their health impacts. We find that African and global anthropogenic aerosol emission reductions produce the largest decreases in $PM_{2.5}$ over Africa. Comparison between the global and Africa-only experiments indicates that the African emission changes make a substantial contribution to dust feedbacks. However, differences in sign and magnitude between the experiments are evident and influence the resulting health impacts. Anthropogenic aerosol emission reductions in the U.S. and Europe also lower African $PM_{2.5}$ through remote teleconnections that enhance Sahel and Sahara rainfall, as well as through long-range transport of aerosols into Northern Africa from Europe.

Substantial inter-model variability in dust emission responses and $PM_{2.5}$ changes highlights the differences in meteorological responses to the anthropogenic aerosol emission reductions and dust emission parameterizations among models. An important open question raised by our results is the origin of this large inter-model spread. Specifically, it is unclear whether model diversity primarily reflects differences in the meteorological response to anthropogenic aerosol reductions or structural differences in dust emission parameterizations. The current RAMIP design does not provide the targeted experiments needed to disentangle these factors, and therefore we cannot attribute the spread quantitatively. Nevertheless, the question has major implications for dust modeling and highlights the need for coordinated experiments in which models are forced with common meteorology (e.g., relaxation to MMM winds) to isolate parameterization differences.

In GISS, the combination of dry convective velocity scale, threshold velocity, precipitation, and surface wind speed explains up to 90% of dust emission variability across regions in Africa. The regression analysis highlights that much of the dust response to anthropogenic aerosol reductions is driven by changes in wind gustiness, a mechanism represented explicitly in GISS but absent in most other CMIP-class models. Soil moisture also plays an important role through its effect on threshold velocity; however, many models likely overestimate moisture persistence, delaying the resumption of dust emissions after rainfall. Overall, these results underscore the value of the GISS regression analysis as a physically interpretable framework for understanding MMM dust and $PM_{2.5}$ anomalies, while cautioning that the quantitative coefficients may not directly transfer to other models due to differences in parameterizations and meteorological responses. Inter-model differences, particularly the distinctive behavior of GISS between the Global and AFR experiments, highlight structural uncertainties in dust–aerosol–climate feedbacks across the ensemble. Also, our analysis suggests that future dust modeling efforts would benefit from incorporating explicit representations of wind gustiness and their sensitivity to climate change, as well as improved treatment of soil moisture dynamics.

Changes in continental-mean dust emissions due to regional and global anthropogenic aerosol reductions are relatively modest (-1.8% to $+2.7\%$); however, the intensity of emissions within dust source regions responds much more strongly, with fractional changes reaching $\pm 30\%$ in the Sahara and $\pm 25\%$ in the Namib, depending on the model and perturbation. Regionally, dust accounts for up to 70% of total $PM_{2.5}$ changes in major source areas such as the Sahara and Namib deserts, and can either offset or amplify the benefits of anthropogenic $PM_{2.5}$ reductions elsewhere. As a result, large anthropogenic aerosol emission reductions do not always lead to uniform health gains for the African continent. Under AFR reductions, dust-related mortality produces no net continental effect, while under Global reductions, dust contributes a small fraction (3.4%) of $PM_{2.5}$-related mortality benefits. These differences arise because mortality impacts depend on local dust concentration changes weighted by the population exposed. In NAE anthropogenic aerosol reductions, dust mortality can offset up to 45% of $PM_{2.5}$ health benefits of remote anthropogenic emission reductions. However, these remote benefits are small and not robust across models. Despite these dust-related offsets in some regions, non-dust $PM_{2.5}$ remains the primary driver of $PM_{2.5}$-related mortality across most of Africa in both the baseline and emission reduction scenarios.

Uncertainties in dust-related mortality are large, with estimated errors often exceeding the mean values. Inter-model spread dominates total uncertainty, contributing roughly 70%–80%, while relative risk function uncertainty accounts for about 20%–30%. Future work should prioritize improving the representation of dust and aerosol processes in climate models to reduce inter-model spread and increase confidence in projections of dust-related health impacts.

By isolating the effect of emission changes while holding population, age distribution, and baseline mortality constant at the SSP3 2050 level, this study quantifies the direct health impact of anthropogenic aerosol emission reductions, providing a benchmark for evaluating future mitigation strategies. Our findings emphasize that effective air quality improvements in Africa require integrated approaches that consider both anthropogenic sources and natural-source feedbacks. More broadly, the study underscores the importance of incorporating meteorological feedbacks into air quality and climate policy planning, as these feedbacks can modulate the expected health benefits of anthropogenic emission reductions, even if the contribution of dust $PM_{2.5}$ remains small and highly uncertain.

Conflict of Interest

The authors declare no conflicts of interest relevant to this study.

Availability Statement

The processed data and code used to generate the main figures are publicly available at Figshare (https://doi.org/10.6084/m9.figshare.31567246; Amooli et al., 2026).

The raw RAMIP individual model outputs used in this study are available at the CEDA Archive:

- GISS-E2-1-G: https://catalogue.ceda.ac.uk/uuid/ffc25e6de67b4e3caa4693a093fd7bab/
- CESM2: https://catalogue.ceda.ac.uk/uuid/b7c87e4dafcc486ba1eca2abac752abf/
- EC-Earth3-AerChem: https://catalogue.ceda.ac.uk/uuid/d581329422fb455ab9af0ea96c04d266/
- NorESM2-LM: https://catalogue.ceda.ac.uk/uuid/44100d99d120487284d7b778dbc76bdf/
- MRI-ESM2-0: https://catalogue.ceda.ac.uk/uuid/e8678aaf39144d8cb10cd02e8a562101/
- CNRM-ESM2-1: https://catalogue.ceda.ac.uk/uuid/5477e60b209a4e169ca60d7f01a017eb/
- CanESM5-1: https://catalogue.ceda.ac.uk/uuid/a33a7cc2d0a84e27a78b24d70fe257e4/
- UKESM1-0-LL: https://catalogue.ceda.ac.uk/uuid/63233813672245a2ba3c6de90c4cfaee/

The gridded SSP population data are available from the NASA SEDAC Population Data sets (https://sedac.ciesin.columbia.edu/data/collection/gpw-v4). The SSP total population by age projections are provided by IIASA (https://iiasa.ac.at/models-tools-data/ssp-2023), and the projected baseline mortality data can be accessed through the GBD Foresight platform (https://vizhub.healthdata.org/gbd-foresight/). The RR data are from Chowdhury et al. (2022).

Acknowledgments
This work was supported by the National Science Foundation Office of International Science and Engineering (OISE), Award Number 2020677, and the Columbia Center for Climate and Life (JAA, DMW). This work was also supported by the University of Reading Advancing the Frontiers of Earth System Prediction (AFESP) Programme (award number A3720200). The authors acknowledge the UK environmental science supercomputer *JASMIN* and the Lamont-Doherty Earth Observatory computing server *Harmattan* for providing the computational environment for data storage and analysis. The NorESM-LM simulations were enabled by resources provided by the National Academic Infrastructure for Supercomputing in Sweden (NAISS), partially funded by the Swedish Research Council through Grant 2022–06725. For the GISS simulations, resources supporting this work were provided by the NASA High-End Computing (HEC) Program through the NASA Center for Climate Simulation (NCCS) at Goddard Space Flight Center. Naga Oshima was supported by the Environment Research and Technology Development Fund (JPMEERF20232001) of the Environmental Restoration and Conservation Agency provided by Ministry of the Environment of Japan, the Arctic Challenge for Sustainability 3 (ArCS-3) (JPMXD1720251001), and a grant for the Global Environmental Research Coordination System from Ministry of the Environment of Japan (MLIT2253). BHS, MTL and LJW acknowledge funding by the Research Council of Norway through Grant 324182 (CATHY), and the European Union through Grant 101137639 (CleanCloud). MTL and BHS also acknowledge funding by the Research Council of Norway through Grant 324556 (ARIDITY). We also acknowledge support by the Center for Advanced Study in Oslo, Norway, which funded and hosted the HETCLIF center during the academic year of 2023/24.

References

Aboagye-Okyere, A., Meidan, D., Hamilton, D. S., Hess, P., Kalashnikova, O., Garay, M., & Mahowald, N. M. (2025). The changing role of dust and open fires PM2.5 on Africa's air quality and human health. *Environmental Research Letters*, *20*(9), 094013. https://doi.org/10.1088/1748-9326/adf07e

Adebiyi, A. A., & Kok, J. F. (2020). Climate models miss most of the coarse dust in the atmosphere. *Science Advances*, *6*(15), eaaz9507. https://doi.org/10.1126/sciadv.aaz9507

Ahn, H.-J., Park, S.-U., & Chang, L.-S. (2007). Effect of direct radiative forcing of Asian dust on the meteorological fields in East Asia during an Asian dust event period. *Journal of Applied Meteorology and Climatology*, *46*(10), 1655–1681. https://doi.org/10.1175/JAM2551.1

Albrecht, B. A. (1989). Aerosols, cloud microphysics, and fractional cloudiness. *Science*, *245*(4923), 1227–1230. https://doi.org/10.1126/SCIENCE.245.4923.1227

Ali, E., Xu, W., Xie, L., & Ding, X. (2022). Assessment of aeolian activity in the Bodélé depression, Chad: A dense spatiotemporal time series from Landsat-8 and Sentinel-2 data. *Frontiers in Environmental Science*, *9*, 808802. https://doi.org/10.3389/fenvs.2021.808802

Allen, C. J. T., Washington, R., & Engelstaedter, S. (2013). Dust emission and transport mechanisms in the central Sahara: Fennec ground-based observations from Bordj Badji Mokhtar, June 2011. *Journal of Geophysical Research: Atmospheres*, *118*(12), 6212–6232. https://doi.org/10.1002/jgrd.50534

Allen, R. J., Turnock, S., Nabat, P., Neubauer, D., Lohmann, U., Olivié, D., et al. (2020). Climate and air quality impacts due to mitigation of non-methane near-term climate forcers. *Atmospheric Chemistry and Physics*, *20*(16), 9641–9663. https://doi.org/10.5194/acp-20-9641-2020

Amooli, J. A., Hackman, K. O., Nana, B., & Westervelt, D. M. (2024). Fine particulate air pollution estimation in Ouagadougou using satellite aerosol optical depth and meteorological parameters. *Environmental Sciences: Atmosphere*, *4*(9), 1012–1025. https://doi.org/10.1039/D4EA00057A

Amooli, J. A., Lund, M. T., Chowdhury, S., Myhre, G., Johansen, A. N., Samset, B. H., & Westervelt, D. M. (2025). An uncertain future for the climate and health impacts of anthropogenic aerosols in Africa. *EGUsphere*, 1–32. https://doi.org/10.5194/egusphere-2025-948

Amooli, J. A., Westervelt, D. M., Wilcox, L. J., Samset, B., & Lund, M. T. (2026). RAMIP_Africa_PM_dust_data_and_code [Dataset]. *Figshare*. https://doi.org/10.6084/m9.figshare.31567246

Aryal, Y., & Evans, S. (2023). Dust emission response to precipitation and temperature anomalies under different climatic conditions. *Science of The Total Environment*, *874*, 162335. https://doi.org/10.1016/j.scitotenv.2023.162335

Atkinson, J. D., Murray, B. J., Woodhouse, M. T., Whale, T. F., Baustian, K. J., Carslaw, K. S., et al. (2013). The importance of feldspar for ice nucleation by mineral dust in mixed-phase clouds. *Nature*, *498*(7454), 355–358. https://doi.org/10.1038/nature12278

Bauer, S. E., Im, U., Mezuman, K., & Gao, C. Y. (2019). Desert dust, industrialization, and agricultural fires: Health impacts of outdoor air pollution in Africa. *Journal of Geophysical Research: Atmospheres*, *124*(7), 4104–4120. https://doi.org/10.1029/2018JD029336

Bauer, S. E., Mishchenko, M. I., Lacis, A. A., Zhang, S., Perlwitz, J., & Metzger, S. M. (2007). Do sulfate and nitrate coatings on mineral dust have important effects on radiative properties and climate modeling? *Journal of Geophysical Research*, *112*(D6). https://doi.org/10.1029/2005JD006977

Bauer, S. E., Tsigaridis, K., Faluvegi, G., Kelley, M., Lo, K. K., Miller, R. L., et al. (2020). Historical (1850–2014) aerosol evolution and role on climate forcing using the GISS ModelE2.1 contribution to CMIP6. *Journal of Advances in Modeling Earth Systems*, *12*(8), e2019MS001978. https://doi.org/10.1029/2019MS001978

Bauer, S. E., Tsigaridis, K., Faluvegi, G., Nazarenko, L., Miller, R. L., Kelley, M., & Schmidt, G. (2022). The turning point of the aerosol era. *Journal of Advances in Modeling Earth Systems*, *14*(12), e2022MS003070. https://doi.org/10.1029/2022MS003070

Bond, T. C., Doherty, S. J., Fahey, D. W., Forster, P. M., Berntsen, T., DeAngelo, B. J., et al. (2013). Bounding the role of black carbon in the climate system: A scientific assessment. *Journal of Geophysical Research: Atmospheres*, *118*(11), 5380–5552. https://doi.org/10.1002/jgrd.50171

Brey, S. J., Pierce, J. R., Barnes, E. A., & Fischer, E. V. (2020). Estimating the spread in future fine dust concentrations in the Southwest United States. *Journal of Geophysical Research: Atmospheres*, *125*(21), e2019JD031735. https://doi.org/10.1029/2019JD031735

Burnett, R., Chen, H., Szyszkowicz, M., Fann, N., Hubbell, B., Pope, C. A., et al. (2018). Global estimates of mortality associated with longterm exposure to outdoor fine particulate matter. *Proceedings of the National Academy of Sciences of the United States of America*, *115*(38), 9592–9597. https://doi.org/10.1073/pnas.1803222115

Cakmur, R. V., Miller, R. L., Perlwitz, J., Geogdzhayev, I. V., Ginoux, P., Koch, D., et al. (2006). Constraining the magnitude of the global dust cycle by minimizing the difference between a model and observations. *Journal of Geophysical Research*, *111*(D6). https://doi.org/10.1029/2005JD005791

Carlson, T. N., & Prospero, J. M. (1972). The large-scale movement of Saharan air outbreaks over the Northern equatorial Atlantic. *Journal of Applied Meteorology and Climatology*, *11*(2), 283–297. https://doi.org/10.1175/1520-0450(1972)011<0283:TLSMOS>2.0.CO;2

Caton Harrison, T., Washington, R., & Engelstaedter, S. (2019). A 14-Year climatology of Saharan dust emission mechanisms inferred from automatically tracked plumes. *Journal of Geophysical Research: Atmospheres*, *124*(16), 9665–9690. https://doi.org/10.1029/2019JD030291

Chou, C., Neelin, J. D., Lohmann, U., & Feichter, J. (2005). Local and remote impacts of aerosol climate forcing on tropical precipitation. *Journal of Climate*, *18*(22), 4621–4636. https://doi.org/10.1175/JCLI3554.1

Chowdhury, S., Hänninen, R., Sofiev, M., & Aunan, K. (2024). Fires as a source of annual ambient PM2.5 exposure and chronic health impacts in Europe. *Science of the Total Environment*, *922*, 171314. https://doi.org/10.1016/J.SCITOTENV.2024.171314

Chowdhury, S., Pillarisetti, A., Oberholzer, A., Jetter, J., Mitchell, J., Cappuccilli, E., et al. (2023). A global review of the state of the evidence of household air pollution's contribution to ambient fine particulate matter and their related health impacts. *Environment International*, *173*, 107835. https://doi.org/10.1016/J.ENVINT.2023.107835

Chowdhury, S., Pozzer, A., Dey, S., Klingmueller, K., & Lelieveld, J. (2020). Changing risk factors that contribute to premature mortality from ambient air pollution between 2000 and 2015. *Environmental Research Letters*, *15*(7), 074010. https://doi.org/10.1088/1748-9326/AB8334

Chowdhury, S., Pozzer, A., Haines, A., Klingmüller, K., Münzel, T., Paasonen, P., et al. (2022). Global health burden of ambient PM2.5 and the contribution of anthropogenic black carbon and organic aerosols. *Environment International*, *159*, 107020. https://doi.org/10.1016/J.ENVINT.2021.107020

Clifford, H. (2019). *A 2000 year Saharan dust event record from a European alps ice core*. The University of Maine.

Cohen, A. J., Brauer, M., Burnett, R., Anderson, H. R., Frostad, J., Estep, K., et al. (2017). Estimates and 25-year trends of the global burden of disease attributable to ambient air pollution: An analysis of data from the global burden of diseases study 2015. *The Lancet*, *389*(10082), 1907–1918. https://doi.org/10.1016/S0140-6736(17)30505-6

Cowie, S. M., Knippertz, P., & Marsham, J. H. (2013). Are vegetation-related roughness changes the cause of the recent decrease in dust emission from the Sahel? *Geophysical Research Letters*, *40*(9), 1868–1872. https://doi.org/10.1002/grl.50273

Danabasoglu, G., Lamarque, J. F., Bacmeister, J., Bailey, D. A., DuVivier, A. K., Edwards, J., et al. (2020). The community Earth system model version 2 (CESM2). *Journal of Advances in Modeling Earth Systems*, *12*(2), e2019MS001916. https://doi.org/10.1029/2019MS001916

Dong, B., Sutton, R. T., Highwood, E., & Wilcox, L. (2014). The impacts of European and Asian anthropogenic sulfur dioxide emissions on Sahel rainfall. *Journal of Climate*, *27*(18), 7000–7017. https://doi.org/10.1175/JCLI-D-13-00769.1

Engelstaedter, S., Tegen, I., & Washington, R. (2006). North African dust emissions and transport. *Earth-Science Reviews*, *79*(1), 73–100. https://doi.org/10.1016/j.earscirev.2006.06.004

Evan, A. T. (2018). Surface winds and dust biases in climate models. *Geophysical Research Letters*, *45*(2), 1079–1085. https://doi.org/10.1002/2017GL076353

Evan, A. T., Flamant, C., Gaetani, M., & Guichard, F. (2016). The past, present and future of African dust. *Nature*, *531*(7595), 493–495. https://doi.org/10.1038/nature17149

Evan, A. T., Vimont, D. J., Heidinger, A. K., Kossin, J. P., & Bennartz, R. (2009). The role of aerosols in the evolution of tropical North Atlantic Ocean temperature anomalies. *Science*, *324*(5928), 778–781. https://doi.org/10.1126/science.1167404

Evans, J., van Donkelaar, A., Martin, R. V., Burnett, R., Rainham, D. G., Birkett, N. J., & Krewski, D. (2013). Estimates of global mortality attributable to particulate air pollution using satellite imagery. *Environmental Research*, *120*, 33–42. https://doi.org/10.1016/j.envres.2012.08.005

Evans, S., Ginoux, P., Malyshev, S., & Shevliakova, E. (2016). Climate-vegetation interaction and amplification of Australian dust variability. *Geophysical Research Letters*, *43*(22), 11823–11830. https://doi.org/10.1002/2016GL071016

Eyring, V., Bony, S., Meehl, G. A., Senior, C. A., Stevens, B., Stouffer, R. J., & Taylor, K. E. (2016). Overview of the Coupled Model Intercomparison Project Phase 6 (CMIP6) experimental design and organization. *Geoscientific Model Development*, *9*(5), 1937–1958. https://doi.org/10.5194/GMD-9-1937-2016

Fan, J., Leung, L. R., DeMott, P. J., Comstock, J. M., Singh, B., Rosenfeld, D., et al. (2014). Aerosol impacts on California winter clouds and precipitation during CalWater 2011: Local pollution versus long-range transported dust. *Atmospheric Chemistry and Physics*, *14*(1), 81–101. https://doi.org/10.5194/acp-14-81-2014

Fang, T., Di, Y., Xu, Y., Shen, N., Fan, H., Hou, S., & Li, X. (2025). Temporal trends of particulate matter pollution and its health burden, 1990-2021, with projections to 2036: A systematic analysis for the global burden of disease study 2021. *Frontiers in Public Health*, *13*, 1579716. https://doi.org/10.3389/fpubh.2025.1579716

Fécan, F., Marticorena, B., & Bergametti, G. (1999). Parametrization of the increase of the aeolian erosion threshold wind friction velocity due to soil moisture for arid and semi-arid areas. *Annales Geophysicae*, *17*(1), 149–157. https://doi.org/10.1007/s00585-999-0149-7

Fiore, A. M., Naik, V., Spracklen, D. V., Steiner, A., Unger, N., Prather, M., et al. (2012). Global air quality and climate. *Chemical Society Reviews*, *41*(19), 6663–6683. https://doi.org/10.1039/C2CS35095E

Garcia-Carreras, L., Marsham, J. H., Stratton, R. A., & Tucker, S. (2021). Capturing convection essential for projections of climate change in African dust emission. *Npj Climate and Atmospheric Science*, *4*(1), 44. https://doi.org/10.1038/s41612-021-00201-x

Garrison, V. H., Majewski, M. S., Konde, L., Wolf, R. E., Otto, R. D., & Tsuneoka, Y. (2014). Inhalable desert dust, urban emissions, and potentially biotoxic metals in urban Saharan–Sahelian air. *Science of the Total Environment*, *500–501*, 383–394. https://doi.org/10.1016/j.scitotenv.2014.08.106

GBD, V.-G. (2024). GBD. Retrieved from https://vizhub.healthdata.org/gbd-results/

Giannadaki, D., Pozzer, A., & Lelieveld, J. (2014). Modeled global effects of airborne desert dust on air quality and premature mortality. *Atmospheric Chemistry and Physics*, *14*(2), 957–968. https://doi.org/10.5194/acp-14-957-2014

Ginoux, P., Chin, M., Tegen, I., Prospero, J. M., Holben, B., Dubovik, O., & Lin, S.-J. (2001). Sources and distributions of dust aerosols simulated with the GOCART model. *Journal of Geophysical Research*, *106*(D17), 20255–20273. https://doi.org/10.1029/2000JD000053

Giordano, M. R., Malings, C., Pandis, S. N., Presto, A. A., McNeill, V. F., Westervelt, D. M., et al. (2021). From low-cost sensors to high-quality data: A summary of challenges and best practices for effectively calibrating low-cost particulate matter mass sensors. *Journal of Aerosol Science*, *158*, 105833. https://doi.org/10.1016/j.jaerosci.2021.105833

Gomez, J., Allen, R. J., Turnock, S. T., Horowitz, L. W., Tsigaridis, K., Bauer, S. E., et al. (2023). The projected future degradation in air quality is caused by more abundant natural aerosols in a warmer world. *Communications Earth & Environment*, *4*(1), 22. https://doi.org/10.1038/s43247-023-00688-7

Grineski, S. E., Staniswalis, J. G., Bulathsinhala, P., Peng, Y., & Gill, T. E. (2011). Hospital admissions for asthma and acute bronchitis in El Paso, Texas: Do age, sex, and insurance status modify the effects of dust and low wind events? *Environmental Research*, *111*(8), 1148–1155. https://doi.org/10.1016/j.envres.2011.06.007

Guo, J., Xie, X., Myhre, G., Shindell, D., Kirkevåg, A., Iversen, T., et al. (2024). Increased Asian sulfate aerosol emissions remarkably enhance Sahel summer precipitation. *Earth's Future*, *12*(11), e2024EF004745. https://doi.org/10.1029/2024EF004745

Heinold, B., Helmert, J., Hellmuth, O., Wolke, R., Ansmann, A., Marticorena, B., et al. (2007). Regional modeling of Saharan dust events using LM-MUSCAT: Model description and case studies. *Journal of Geophysical Research*, *112*(D11). https://doi.org/10.1029/2006JD007443

Heinold, B., Tegen, I., Schepanski, K., & Banks, J. R. (2016). New developments in the representation of Saharan dust sources in the aerosol–climate model ECHAM6-HAM2. *Geoscientific Model Development*, *9*(2), 765–777. https://doi.org/10.5194/gmd-9-765-2016

Hienola, A., Partanen, A.-I., Pietikäinen, J.-P., O'Donnell, D., Korhonen, H., Matthews, H. D., & Laaksonen, A. (2018). The impact of aerosol emissions on the 1.5°C pathways. *Environmental Research Letters*, *13*(4), 044011. https://doi.org/10.1088/1748-9326/aab1b2

Hirasawa, H., Kushner, P. J., Sigmond, M., Fyfe, J., & Deser, C. (2022). Evolving Sahel rainfall response to anthropogenic aerosols driven by shifting regional Oceanic and emission influences. *Journal of Climate*, *35*(11), 3181–3193. https://doi.org/10.1175/JCLI-D-21-0795.1

Huneeus, N., Schulz, M., Balkanski, Y., Griesfeller, J., Prospero, J., Kinne, S., et al. (2011). Global dust model intercomparison in AeroCom phase I. *Atmospheric Chemistry and Physics*, *11*(15), 7781–7816. https://doi.org/10.5194/acp-11-7781-2011

Im, U., Bauer, S. E., Frohn, L. M., Geels, C., Tsigaridis, K., & Brandt, J. (2023). Present-day and future PM2.5 and O_3-related global and regional premature mortality in the EVAv6.0 health impact assessment model. *Environmental Research*, *216*, 114702. https://doi.org/10.1016/j.envres.2022.114702

Im, U., Christensen, J. H., Geels, C., Hansen, K. M., Brandt, J., Solazzo, E., et al. (2018). Influence of anthropogenic emissions and boundary conditions on multi-model simulations of major air pollutants over Europe and North America in the framework of AQMEII3. *Atmospheric Chemistry and Physics*, *18*(12), 8929–8952. https://doi.org/10.5194/acp-18-8929-2018

Jacobson, M. Z., & Kaufman, Y. J. (2006). Wind reduction by aerosol particles. *Geophysical Research Letters*, *33*(24). https://doi.org/10.1029/2006GL027838

Jenkins, G., Tindan, J., & Gebremariam, S. (2025). WRF simulations of future Saharan dust concentrations across West Africa: Historical and late 21st century. *Journal of Geophysical Research: Atmospheres*, *130*(19), e2025JD043892. https://doi.org/10.1029/2025JD043892

Jones, B., O'Neill, B. C., & Gao, J. (2020). Global 1-km downscaled population base year and projection grids based on the shared socioeconomic pathways, revision 01 NASA earthdata [Dataset]. https://www.earthdata.nasa.gov/data/catalog/sedac-ciesin-sedac-pd-sspbsyr-1km-1.01

KC, S., Moradhvaj, Potancokova, M., Adhikari, S., Yildiz, D., Mamolo, M., et al. (2024). Wittgenstein Center (WIC) population and human capital Projections—2023 [Dataset]. *Zenodo*. https://zenodo.org/records/14718294

Kelley, M., Schmidt, G. A., Nazarenko, L. S., Bauer, S. E., Ruedy, R., Russell, G. L., et al. (2020). GISS-E2.1: Configurations and climatology. *Journal of Advances in Modeling Earth Systems*, *12*(8), e2019MS002025. https://doi.org/10.1029/2019MS002025

Kim, D., Chin, M., Bian, H., Tan, Q., Brown, M. E., Zheng, T., et al. (2013). The effect of the dynamic surface bareness on dust source function, emission, and distribution. *Journal of Geophysical Research: Atmospheres*, *118*(2), 871–886. https://doi.org/10.1029/2012JD017907

Kim, D., Chin, M., Remer, L. A., Diehl, T., Bian, H., Yu, H., et al. (2017). Role of surface wind and vegetation cover in multi-decadal variations of dust emission in the Sahara and Sahel. *Atmospheric Environment*, *148*, 282–296. https://doi.org/10.1016/j.atmosenv.2016.10.051

Kloster, S., Dentener, F., Feichter, J., Raes, F., Lohmann, U., Roeckner, E., & Fischer-Bruns, I. (2010). A GCM study of future climate response to aerosol pollution reductions. *Climate Dynamics*, *34*(7), 1177–1194. https://doi.org/10.1007/s00382-009-0573-0

Knippertz, P., & Todd, M. C. (2012). Mineral dust aerosols over the Sahara: Meteorological controls on emission and transport and implications for modeling. *Reviews of Geophysics*, *50*(1). https://doi.org/10.1029/2011RG000362

Kok, J. F. (2011). A scaling theory for the size distribution of emitted dust aerosols suggests climate models underestimate the size of the global dust cycle. *Proceedings of the National Academy of Sciences*, *108*(3), 1016–1021. https://doi.org/10.1073/pnas.1014798108

Kok, J. F., Adebiyi, A. A., Albani, S., Balkanski, Y., Checa-Garcia, R., Chin, M., et al. (2021). Contribution of the world's main dust source regions to the global cycle of desert dust. *Atmospheric Chemistry and Physics*, *21*(10), 8169–8193. https://doi.org/10.5194/acp-21-8169-2021

Kok, J. F., Ridley, D. A., Zhou, Q., Miller, R. L., Zhao, C., Heald, C. L., et al. (2017). Smaller desert dust cooling effect estimated from analysis of dust size and abundance. *Nature Geoscience*, *10*(4), 274–278. https://doi.org/10.1038/ngeo2912

Kok, J. F., Storelvmo, T., Karydis, V. A., Adebiyi, A. A., Mahowald, N. M., Evan, A. T., et al. (2023). Mineral dust aerosol impacts on global climate and climate change. *Nature Reviews Earth & Environment*, *4*(2), 71–86. https://doi.org/10.1038/s43017-022-00379-5

Kok, J. F., Ward, D. S., Mahowald, N. M., & Evan, A. T. (2018). Global and regional importance of the direct dust-climate feedback. *Nature Communications*, *9*(1), 241. https://doi.org/10.1038/s41467-017-02620-y

Lelieveld, J., Evans, J. S., Fnais, M., Giannadaki, D., & Pozzer, A. (2015). The contribution of outdoor air pollution sources to premature mortality on a global scale. *Nature 2015*, *525*(7569), 367–371. https://doi.org/10.1038/nature15371

Lelieveld, J., Klingmüller, K., Pozzer, A., Burnett, R. T., Haines, A., & Ramanathan, V. (2019). Effects of fossil fuel and total anthropogenic emission removal on public health and climate. *Proceedings of the National Academy of Sciences of the United States of America*, *116*(15), 7192–7197. https://doi.org/10.1073/PNAS.1819989116

Leung, D. M., Kok, J. F., Li, L., Lawrence, D. M., Mahowald, N. M., Tilmes, S., & Kluzek, E. (2025). A global dust emission dataset for estimating dust radiative forcings in climate models. *Atmospheric Chemistry and Physics*, *25*(4), 2311–2331. https://doi.org/10.5194/acp-25-2311-2025

Li, J., Yu, H., Kulmala, M., Kokkonen, T. V., Tang, K., Ma, J., et al. (2024). Aerosol forces mesoscale secondary circulations occurrence: Evidence of emission reduction. *Npj Climate and Atmospheric Science*, *7*(1), 306. https://doi.org/10.1038/s41612-024-00868-y

Li, T., Hu, R., Chen, Z., Li, Q., Huang, S., Zhu, Z., & Zhou, L.-F. (2018). Fine particulate matter (PM2.5): The culprit for chronic lung diseases in China. *Chronic Diseases and Translational Medicine*, *4*(3), 176–186. https://doi.org/10.1016/j.cdtm.2018.07.002

Lim, S. S., Vos, T., Flaxman, A. D., Danaei, G., Shibuya, K., Adair-Rohani, H., et al. (2012). A comparative risk assessment of burden of disease and injury attributable to 67 risk factors and risk factor clusters in 21 regions, 1990–2010: A systematic analysis for the global burden of disease study 2010. *The Lancet*, *380*(9859), 2224–2260. https://doi.org/10.1016/S0140-6736(12)61766-8

Liu, W., Li, S., Li, C., Rugenstein, M., & Thomas, A. P. (2024). Contrasting fast and slow intertropical convergence zone migrations linked to delayed Southern Ocean warming. *Nature Climate Change*, *14*(7), 732–739. https://doi.org/10.1038/s41558-024-02034-x

Lund, M. T., Myhre, G., & Samset, B. H. (2019). Anthropogenic aerosol forcing under the shared socioeconomic pathways. *Atmospheric Chemistry and Physics*, *19*(22), 13827–13839. https://doi.org/10.5194/acp-19-13827-2019

Mahowald, N. M., Kloster, S., Engelstaedter, S., Moore, J. K., Mukhopadhyay, S., McConnell, J. R., et al. (2010). Observed 20th century desert dust variability: Impact on climate and biogeochemistry. *Atmospheric Chemistry and Physics*, *10*(22), 10875–10893. https://doi.org/10.5194/acp-10-10875-2010

Mallone, S., Stafoggia, M., Faustini, A., Gobbi, G. P., Marconi, A., & Forastiere, F. (2011). Saharan dust and associations between particulate matter and daily mortality in Rome, Italy. *Environmental Health Perspectives*, *119*(10), 1409–1414. https://doi.org/10.1289/ehp.1003026

Marticorena, B., & Bergametti, G. (1995). Modeling the atmospheric dust cycle: 1. Design of a soil-derived dust emission scheme. *Journal of Geophysical Research*, *100*(D8), 16415–16430. https://doi.org/10.1029/95JD00690

McDuffie, E., Martin, R., Yin, H., & Brauer, M. (2021). *Global burden of disease from major air pollution sources (GBD MAPS): A global approach* (p. 210). Research Reports: Health Effects Institute, 2021. Retrieved from https://www.ncbi.nlm.nih.gov/pmc/articles/PMC9501767/

Miller, R. L., Cakmur, R. V., Perlwitz, J., Geogdzhayev, I. V., Ginoux, P., Koch, D., et al. (2006). Mineral dust aerosols in the NASA Goddard Institute for Space Sciences ModelE atmospheric general circulation model. *Journal of Geophysical Research*, *111*(D6). https://doi.org/10.1029/2005JD005796

Miller, R. L., Knippertz, P., Pérez García-Pando, C., Perlwitz, J. P., & Tegen, I. (2014). Impact of dust radiative forcing upon climate. In P. Knippertz & J.-B. W. Stuut (Eds.), *Mineral dust: A key player in the Earth system* (pp. 327–357). Springer Netherlands. https://doi.org/10.1007/978-94-017-8978-3_13

Miller, R. L., Perlwitz, J., & Tegen, I. (2004). Feedback upon dust emission by dust radiative forcing through the planetary boundary layer. *Journal of Geophysical Research*, *109*(D24). https://doi.org/10.1029/2004JD004912

Miller, R. L., & Tegen, I. (1998). Climate response to soil dust aerosols. *Journal of climate*, *11*(12), 3247–3267. https://doi.org/10.1175/1520-0442(1998)011<3247:CRTSDA>2.0.CO;2

Miller, R. L., Tegen, I., & Perlwitz, J. (2004). Surface radiative forcing by soil dust aerosols and the hydrologic cycle. *Journal of Geophysical Research*, *109*(D4). https://doi.org/10.1029/2003JD004085

Ming, Y., Ramaswamy, V., & Persad, G. (2010). Two opposing effects of absorbing aerosols on global-mean precipitation. *Geophysical Research Letters*, *37*(13). https://doi.org/10.1029/2010GL042895

Monerie, P.-A., Dittus, A. J., Wilcox, L. J., & Turner, A. G. (2023). Uncertainty in simulating twentieth century West African precipitation trends: The role of anthropogenic aerosol emissions. *Earth's Future*, *11*(2), e2022EF002995. https://doi.org/10.1029/2022EF002995

Munson, S. M., Belnap, J., & Okin, G. S. (2011). Responses of wind erosion to climate-induced vegetation changes on the Colorado Plateau. *Proceedings of the National Academy of Sciences*, *108*(10), 3854–3859. https://doi.org/10.1073/pnas.1014947108

Murray, C. J. L., Abbafati, C., Abbas, K. M., Abbasi-Kangevari, M., Abd-Allah, F., Abdelalim, A., et al. (2020). Global burden of 87 risk factors in 204 countries and territories, 1990-2019: A systematic analysis for the global burden of disease study 2019. *Lancet (London, England)*, *396*(10258), 1223–1249. https://doi.org/10.1016/S0140-6736(20)30752-2

Myhre, G., Samset, B. H., Schulz, M., Balkanski, Y., Bauer, S., Berntsen, T. K., et al. (2013). Radiative forcing of the direct aerosol effect from AeroCom phase II simulations. *Atmospheric Chemistry and Physics*, *13*(4), 1853–1877. https://doi.org/10.5194/ACP-13-1853-2013

Navarro, J. C. A., Ekman, A. M. L., Pausata, F. S. R., Lewinschal, A., Varma, V., Seland, Ø., et al. (2017). Future response of temperature and precipitation to reduced aerosol emissions as compared with increased greenhouse gas concentrations. https://doi.org/10.1175/JCLI-D-16-0466.1

Okin, G. S. (2022). Where and how often does rain prevent dust emission? *Geophysical Research Letters*, *49*(4), e2021GL095501. https://doi.org/10.1029/2021GL095501

Ostro, B., Awe, Y., & Sánchez-Triana, E. (2021). When the dust settles: A review of the health implications of the dust component of air pollution. Retrieved from http://hdl.handle.net/10986/36267

Pérez García-Pando, C., Thomson, M., Stanton, M., Diggle, P., Hopson, T., Pandya, R., et al. (2014). Meningitis and climate – From science to practice. *Earth Perspectives - Transdisciplinarity Enabled*, *1*, 14. https://doi.org/10.1186/2194-6434-1-14

Perlwitz, J. P., Pérez García-Pando, C., & Miller, R. L. (2015). Predicting the mineral composition of dust aerosols – Part 1: Representing key processes. *Atmospheric Chemistry and Physics*, *15*(20), 11593–11627. https://doi.org/10.5194/acp-15-11593-2015

Persad, G. G., & Caldeira, K. (2018). Divergent global-scale temperature effects from identical aerosols emitted in different regions. *Nature Communications*, *9*(1), 3289. https://doi.org/10.1038/s41467-018-05838-6

Pope, C. A., Burnett, R. T., Thun, M. J., Calle, E. E., Krewski, D., Ito, K., & Thurston, G. D. (2002). Lung cancer, cardiopulmonary mortality, and long-term exposure to fine particulate air pollution. *JAMA*, *287*(9), 1132–1141. https://doi.org/10.1001/JAMA.287.9.1132

Pozzer, A., Anenberg, S. C., Dey, S., Haines, A., Lelieveld, J., & Chowdhury, S. (2023). Mortality attributable to ambient air pollution: A review of global estimates. *GeoHealth*, *7*(1), e2022GH000711. https://doi.org/10.1029/2022GH000711

Proestakis, E., Papachristopoulou, K., Georgiou, T., Chatoutsidou, S. E., Lazaridis, M., Gkikas, A., et al. (2025). *Atmospheric dust and air quality over large-cities and megacities of the world* (pp. 1–58). EGUsphere. https://doi.org/10.5194/egusphere-2025-1841

Prospero, J. M. (1999). Long-term measurements of the transport of African mineral dust to the southeastern United States: Implications for regional air quality. *Journal of Geophysical Research*, *104*(D13), 15917–15927. https://doi.org/10.1029/1999JD900072

Prospero, J. M., & Lamb, P. J. (2003). African droughts and dust transport to the Caribbean: Climate change implications. *Science*, *302*(5647), 1024–1027. https://doi.org/10.1126/science.1089915

Pu, B., & Ginoux, P. (2017). Projection of American dustiness in the late 21st century due to climate change. *Scientific Reports*, *7*(1), 5553. https://doi.org/10.1038/s41598-017-05431-9

Pu, B., & Ginoux, P. (2018). How reliable are CMIP5 models in simulating dust optical depth? *Atmospheric Chemistry and Physics*, *18*(16), 12491–12510. https://doi.org/10.5194/acp-18-12491-2018

Querol, X., Tobías, A., Pérez, N., Karanasiou, A., Amato, F., Stafoggia, M., et al. (2019). Monitoring the impact of desert dust outbreaks for air quality for health studies. *Environment International*, *130*, 104867. https://doi.org/10.1016/J.ENVINT.2019.05.061

Ramanathan, V., Crutzen, P. J., Kiehl, J. T., & Rosenfeld, D. (2001). Aerosols, climate, and the hydrological cycle. *Science*, *294*(5549), 2119–2124. https://doi.org/10.1126/science.1064034

Ran, Q., Moore, J., Dong, T., Lee, S.-Y., & Dong, W. (2023). Statistical bias correction for CESM-simulated PM 2.5. *Environmental Research Communications*, *5*(10), 101001. https://doi.org/10.1088/2515-7620/acf917

Rao, S., Klimont, Z., Smith, S. J., Dingenen, R. V., Dentener, F., Bouwman, L., et al. (2017). Future air pollution in the shared Socio-economic pathways. *Global Environmental Change*, *42*, 346–358. https://doi.org/10.1016/J.GLOENVCHA.2016.05.012

Riahi, K., van Vuuren, D. P., Kriegler, E., Edmonds, J., O'Neill, B. C., Fujimori, S., et al. (2017). The shared socioeconomic pathways and their energy, land use, and greenhouse gas emissions implications: An overview. *Global Environmental Change*, *42*, 153–168. https://doi.org/10.1016/J.GLOENVCHA.2016.05.009

Ridley, D. A., Heald, C. L., & Ford, B. (2012). North African dust export and deposition: A satellite and model perspective. *Journal of Geophysical Research*, *117*(D2). https://doi.org/10.1029/2011JD016794

Rosenfeld, D., Rudich, Y., & Lahav, R. (2001). Desert dust suppressing precipitation: A possible desertification feedback loop. *Proceedings of the National Academy of Sciences*, *98*(11), 5975–5980. https://doi.org/10.1073/pnas.101122798

Rotstayn, L. D., Collier, M. A., Chrastansky, A., Jeffrey, S. J., & Luo, J.-J. (2013). Projected effects of declining aerosols in RCP4.5: Unmasking global warming? *Atmospheric Chemistry and Physics*, *13*(21), 10883–10905. https://doi.org/10.5194/acp-13-10883-2013

Salzmann, M. (2016). Global warming without global mean precipitation increase? *Science Advances*, *2*(6), e1501572. https://doi.org/10.1126/sciadv.1501572

Samset, B. H., Sand, M., Smith, C. J., Bauer, S. E., Forster, P. M., Fuglestvedt, J. S., et al. (2018). Climate impacts from a removal of anthropogenic aerosol emissions. *Geophysical Research Letters*, *45*(2), 1020–1029. https://doi.org/10.1002/2017GL076079

Samset, B. H., Wilcox, L. J., Allen, R. J., Stjern, C. W., Lund, M. T., Ahmadi, S., et al. (2025). East Asian aerosol cleanup has likely contributed to the recent acceleration in global warming. *Communications Earth & Environment*, *6*(1), 543. https://doi.org/10.1038/s43247-025-02527-3

Scannell, C., Booth, B. B. B., Dunstone, N. J., Rowell, D. P., Bernie, D. J., Kasoar, M., et al. (2019). The influence of remote aerosol forcing from industrialized economies on the future evolution of east and West African rainfall. *Journal of Climate*, *32*(23), 8335–8354. https://doi.org/10.1175/JCLI-D-18-0716.1

Séférian, R., Nabat, P., Michou, M., Saint-Martin, D., Voldoire, A., Colin, J., et al. (2019). Evaluation of CNRM earth system model, CNRM-ESM2-1: Role of Earth system processes in present-day and future climate. *Journal of Advances in Modeling Earth Systems*, *11*(12), 4182–4227. https://doi.org/10.1029/2019MS001791

Seland, Ø., Bentsen, M., Olivié, D., Toniazzo, T., Gjermundsen, A., Graff, L. S., et al. (2020). Overview of the Norwegian Earth system model (NorESM2) and key climate response of CMIP6 DECK, historical, and scenario simulations. *Geoscientific Model Development*, *13*(12), 6165–6200. https://doi.org/10.5194/GMD-13-6165-2020

Sellar, A., Jones, C., Mulcahy, J., Tang, Y., Yool, A., Wiltshire, A., et al. (2019). UKESM1: Description and evaluation of the UK Earth system model. *Journal of Advances in Modeling Earth Systems*, *11*(12), 4513–4558. https://doi.org/10.1029/2019MS001739

Shindell, D., Faluvegi, G., Parsons, L., Nagamoto, E., & Chang, J. (2022). Premature deaths in Africa due to particulate matter under high and low warming scenarios. *GeoHealth*, *6*(5), e2022GH000601. https://doi.org/10.1029/2022GH000601

Shindell, D., Parsons, L., Faluvegi, G., Hicks, K., Kuylenstierna, J., & Heaps, C. (2023). The important role of African emissions reductions in projected local rainfall changes. *npj Climate and Atmospheric Science*, *6*(1), 47. https://doi.org/10.1038/s41612-023-00382-7

Shindell, D., & Smith, C. J. (2019). Climate and air-quality benefits of a realistic phase-out of fossil fuels. *Nature*, *573*(7774), 408–411. https://doi.org/10.1038/s41586-019-1554-z

Shindell, D. T., Voulgarakis, A., Faluvegi, G., & Milly, G. (2012). Precipitation response to regional radiative forcing. *Atmospheric Chemistry and Physics*, *12*(15), 6969–6982. https://doi.org/10.5194/acp-12-6969-2012

Southerland, V. A., Brauer, M., Mohegh, A., Hammer, M. S., van Donkelaar, A., Martin, R. V., et al. (2022). Global urban temporal trends in fine particulate matter (PM2·5) and attributable health burdens: Estimates from global datasets. *The Lancet Planetary Health*, *6*(2), e139–e146. https://doi.org/10.1016/S2542-5196(21)00350-8

Stafoggia, M., Samoli, E., Alessandrini, E., Cadum, E., Ostro, B., Berti, G., et al. (2013). Short-term associations between fine and coarse particulate matter and hospitalizations in Southern Europe: Results from the MED-PARTICLES Project. *Environmental Health Perspectives*, *121*(9), 1026–1033. https://doi.org/10.1289/ehp.1206151

Stier, P., van den Heever, S. C., Christensen, M. W., Gryspeerdt, E., Dagan, G., Saleeby, S. M., et al. (2024). Multifaceted aerosol effects on precipitation. *Nature Geoscience*, *17*(8), 719–732. https://doi.org/10.1038/s41561-024-01482-6

Stjern, C. W., Hodnebrog, Ø., Myhre, G., & Pisso, I. (2023). The turbulent future brings a breath of fresh air. *Nature Communications*, *14*(1), 3735. https://doi.org/10.1038/s41467-023-39298-4

Swart, N. C., Cole, J. N. S., Kharin, V. V., Lazare, M., Scinocca, J. F., Gillett, N. P., et al. (2019). The Canadian Earth System Model version 5 (CanESM5.0.3). *Geoscientific Model Development*, *12*(11), 4823–4873. https://doi.org/10.5194/gmd-12-4823-2019

Tanaka, T. Y., & Chiba, M. (2005). Global simulation of dust aerosol with a chemical transport model, MASINGAR. *Journal of the Meteorological Society of Japan. Series II*, *83A*, 255–278. https://doi.org/10.2151/jmsj.83A.255

Textor, C., Schulz, M., Guibert, S., Kinne, S., Balkanski, Y., Bauer, S., et al. (2006). Analysis and quantification of the diversities of aerosol life cycles within AeroCom. *Atmospheric Chemistry and Physics*, *6*(7), 1777–1813. https://doi.org/10.5194/acp-6-1777-2006

Toolan, C., Turner, A., & Amooli, J. A. (2025). Sub-Saharan African precipitation responses to aerosol emission changes (Nos. EGU25-6953). *Copernicus Meetings*, EGU25. https://doi.org/10.5194/egusphere-egu25-6953

Toolan, C. A., Amooli, J. A., Wilcox, L. J., Samset, B. H., Turner, A. G., & Westervelt, D. M. (2024). Strong inter-model differences and biases in CMIP6 simulations of PM $_{2.5}$, aerosol optical depth, and precipitation over Africa. https://doi.org/10.5194/EGUSPHERE-2024-3057

Toolan, C. A., Amooli, J. A., Wilcox, L. J., Samset, B. H., Turner, A. G., & Westervelt, D. M. (2025). Strong intermodel differences and biases in CMIP6 simulations of $PM_{2.5}$, aerosol optical depth, and precipitation over Africa. *Atmospheric Chemistry and Physics*, *25*(18), 10523–10557. https://doi.org/10.5194/acp-25-10523-2025

Tsigaridis, K., Daskalakis, N., Kanakidou, M., Adams, P. J., Artaxo, P., Bahadur, R., et al. (2014). The AeroCom evaluation and intercomparison of organic aerosol in global models. *Atmospheric Chemistry and Physics*, *14*(19), 10845–10895. https://doi.org/10.5194/acp-14-10845-2014

Turnock, S. T., Allen, R. J., Andrews, M., Bauer, S. E., Deushi, M., Emmons, L., et al. (2020). Historical and future changes in air pollutants from CMIP6 models. *Atmospheric Chemistry and Physics*, *20*(23), 14547–14579. https://doi.org/10.5194/ACP-20-14547-2020

Undorf, S., Polson, D., Bollasina, M. A., Ming, Y., Schurer, A., & Hegerl, G. C. (2018). Detectable impact of local and remote anthropogenic aerosols on the 20th century changes of West African and South Asian monsoon precipitation. *Journal of Geophysical Research: Atmospheres*, *123*(10), 4871–4889. https://doi.org/10.1029/2017JD027711

van Noije, T., Bergman, T., Le Sager, P., O'Donnell, D., Makkonen, R., Gonçalves-Ageitos, M., et al. (2021). EC-Earth3-AerChem: A global climate model with interactive aerosols and atmospheric chemistry participating in CMIP6. *Geoscientific Model Development*, *14*(9), 5637–5668. https://doi.org/10.5194/gmd-14-5637-2021

van Vuuren, D. P., Edmonds, J., Kainuma, M., Riahi, K., Thomson, A., Hibbard, K., et al. (2011). The representative concentration pathways: An overview. *Climatic Change*, *109*(1), 5–31. https://doi.org/10.1007/s10584-011-0148-z

Vautard, R., Cattiaux, J., Yiou, P., Thépaut, J.-N., & Ciais, P. (2010). Northern Hemisphere atmospheric stilling partly attributed to an increase in surface roughness. *Nature Geoscience*, *3*(11), 756–761. https://doi.org/10.1038/ngeo979

Wang, N., & Zhang, Y. (2024). Long-term variations of global dust emissions and climate control. *Environmental Pollution*, *340*, 122847. https://doi.org/10.1016/j.envpol.2023.122847

Wang, X., Wang, Q., Prass, M., Pöhlker, C., Moran-Zuloaga, D., Artaxo, P., et al. (2023). The export of African mineral dust across the Atlantic and its impact over the Amazon Basin. *Atmospheric Chemistry and Physics*, *23*(17), 9993–10014. https://doi.org/10.5194/acp-23-9993-2023

Weagle, C. L., Snider, G., Li, C., van Donkelaar, A., Philip, S., Bissonnette, P., et al. (2018). Global sources of fine particulate matter: Interpretation of PM2.5 chemical composition observed by Spartan using a global chemical transport model. *Environmental Science & Technology*, *52*(20), 11670–11681. https://doi.org/10.1021/acs.est.8b01658

Wells, C. D., Kasoar, M., Ezzati, M., & Voulgarakis, A. (2024). Significant human health co-benefits of mitigating African emissions. *Atmospheric Chemistry and Physics*, *24*(2), 1025–1039. https://doi.org/10.5194/ACP-24-1025-2024

Westervelt, D. M., Amooli, J. A., & Anand, A. (2025). Twenty years of high spatiotemporal resolution estimates of daily PM2.5 in West Africa using satellite data, surface monitors, and machine learning. *ACS ES&T Air*, *2*(8), 1468–1477. https://doi.org/10.1021/ACSESTAIR.4C00366

Westervelt, D. M., Conley, A. J., Fiore, A. M., Lamarque, J. F., Shindell, D., Previdi, M., et al. (2017). Multimodel precipitation responses to removal of U.S. sulfur dioxide emissions. *Journal of Geophysical Research: Atmospheres*, *122*(9), 5024–5038. https://doi.org/10.1002/2017JD026756

Westervelt, D. M., Conley, A. J., Fiore, A. M., Lamarque, J. F., Shindell, D. T., Previdi, M., et al. (2018). Connecting regional aerosol emissions reductions to local and remote precipitation responses. *Atmospheric Chemistry and Physics*, *18*(16), 12461–12475. https://doi.org/10.5194/ACP-18-12461-2018

Westervelt, D. M., Horowitz, L. W., Naik, V., Tai, A. P. K., Fiore, A. M., & Mauzerall, D. L. (2016). Quantifying PM2.5-meteorology sensitivities in a global climate model. *Atmospheric Environment*, *142*, 43–56. https://doi.org/10.1016/J.ATMOSENV.2016.07.040

Westervelt, D. M., Horowitz, L. W., Naik, V., Golaz, J. C., & Mauzerall, D. L. (2015). Radiative forcing and climate response to projected 21st century aerosol decreases. *Atmospheric Chemistry and Physics*, *15*(22), 12681–12703. https://doi.org/10.5194/ACP-15-12681-2015

Wilcox, L. J., Allen, R. J., Samset, B. H., Bollasina, M. A., Griffiths, P. T., Keeble, J., et al. (2023). The regional aerosol model intercomparison project (RAMIP). *Geoscientific Model Development*, *16*(15), 4451–4479. https://doi.org/10.5194/GMD-16-4451-2023

Woodward, S. (2001). Modeling the atmospheric life cycle and radiative impact of mineral dust in the Hadley Centre climate model. *Journal of Geophysical Research*, *106*(D16), 18155–18166. https://doi.org/10.1029/2000JD900795

Wu, C., Lin, Z., & Liu, X. (2020). The global dust cycle and uncertainty in CMIP5 (Coupled Model Intercomparison Project phase 5) models. *Atmospheric Chemistry and Physics*, *20*(17), 10401–10425. https://doi.org/10.5194/acp-20-10401-2020

Wu, P., Christidis, N., & Stott, P. (2013). Anthropogenic impact on Earth's hydrological cycle. *Nature Climate Change*, *3*(9), 807–810. https://doi.org/10.1038/nclimate1932

Yang, A., Tan, Q., Rajapakshe, C., Chin, M., & Yu, H. (2022). Global premature mortality by dust and pollution PM2.5 estimated from aerosol reanalysis of the modern-era retrospective analysis for research and applications, version 2. *Frontiers in Environmental Science*, *10*, 975755. https://doi.org/10.3389/fenvs.2022.975755

Yukimoto, S., Kawai, H., Koshiro, T., Oshima, N., Yoshida, K., URAKAWA, S., et al. (2019). The meteorological research Institute Earth system model version 2.0, MRI-ESM2.0: Description and basic evaluation of the physical component. *Journal of the Meteorological Society of Japan*, *97*(5), 931–965. https://doi.org/10.2151/jmsj.2019-051

Zender, C. S., Bian, H., & Newman, D. (2003). Mineral dust entrainment and deposition (DEAD) model: Description and 1990s dust climatology. *Journal of Geophysical Research*, *108*(D14). https://doi.org/10.1029/2002JD002775

Zender, C. S., & Kwon, E. Y. (2005). Regional contrasts in dust emission responses to climate. *Journal of Geophysical Research*, *110*(D13). https://doi.org/10.1029/2004JD005501

Zhang, Y., Yu, F., Luo, G., Fan, J., & Liu, S. (2021). Impacts of long-range-transported mineral dust on summertime convective cloud and precipitation: A case study over the Taiwan region. *Atmospheric Chemistry and Physics*, *21*(23), 17433–17451. https://doi.org/10.5194/acp-21-17433-2021

Zhao, A., Ryder, C. L., & Wilcox, L. J. (2022). How well do the CMIP6 models simulate dust aerosols? *Atmospheric Chemistry and Physics*, *22*(3), 2095–2119. https://doi.org/10.5194/acp-22-2095-2022

Zhao, X., Allen, R. J., & Thomson, E. S. (2021). An implicit air quality bias due to the state of pristine aerosol. *Earth's Future*, *9*(9), e2021EF001979. https://doi.org/10.1029/2021EF001979

Zhu, L., Wang, Y., Chavas, D., Johncox, M., & Yung, Y. L. (2024). Leading role of Saharan dust on tropical cyclone rainfall in the Atlantic Basin. *Science Advances*, *10*(30), eadn6106. https://doi.org/10.1126/sciadv.adn6106